Genome-wide screen identifies host loci that modulate *M. tuberculosis* fitness in immunodivergent mice

Short title: *M. tuberculosis* TnSeq in BXD mice

Authors:

Rachel K. Meade[a,b], Jarukit E. Long[c,d], Adrian Jinich[e], Kyu Y. Rhee[e], David G. Ashbrook[f], Robert W. Williams[f], Christopher M. Sassetti[c], Clare M. Smith[a,b*]

Affiliations:

[a] Department of Molecular Genetics and Microbiology, Duke University, Durham, NC, USA

[b] University Program in Genetics and Genomics, Duke University, Durham, NC, USA

[c] Department of Microbiology and Physiological Systems, UMass Chan Medical School, Worcester, MA, USA

[d] Charles River Laboratories, Research Animal Diagnostic Services, Wilmington, MA, USA

[e] Division of Infectious Diseases, Weill Cornell Medical College, NY, USA

[f] Department of Genetics, Genomics and Informatics, University of Tennessee Health Science Center, Memphis, TN, USA

*Correspondence to Clare M. Smith at clare.m.smith@duke.edu

Keywords: Host-pathogen interactions, tuberculosis, mycobacteria, systems genetics, genomics, genetic diversity, natural variation, bacterial genetics, TnSeq, mouse models, BXD, QTL mapping, complex traits

Abstract: Genetic differences among mammalian hosts and *Mycobacterium tuberculosis* (*Mtb*) strains determine diverse tuberculosis (TB) patient outcomes. The advent of recombinant inbred mouse panels and next-generation transposon mutagenesis and sequencing approaches has enabled dissection of complex host-pathogen interactions. To identify host and pathogen genetic determinants of *Mtb* pathogenesis, we infected members of the BXD family of mouse strains with a comprehensive library of *Mtb* transposon mutants (TnSeq). Members of the BXD family segregate for *Mtb*-resistant C57BL/6J (B6 or *B*) and *Mtb*-susceptible DBA/2J (D2 or *D*) haplotypes. The survival of each bacterial mutant was quantified within each BXD host, and we identified those bacterial genes that were differentially required for *Mtb* fitness across BXD genotypes. Mutants that varied in survival among the host family of strains were leveraged as reporters for “endophenotypes”, each bacterial fitness profile directly probing specific components of the infection microenvironment. We conducted QTL mapping of these bacterial fitness endophenotypes and identified 140 *host-pathogen* quantitative trait loci (*hp*QTL). We identified a QTL hotspot on chromosome 6 (75.97–88.58 Mb) associated with the genetic requirement of multiple *Mtb* genes; *Rv0127* (*mak*), *Rv0359* (*rip2*), *Rv0955* (*perM*), and *Rv3849* (*espR*). Together, this screen reinforces the utility of bacterial mutant libraries as precise reporters of the host

47 immunological microenvironment during infection and highlights specific host-pathogen
48 genetic interactions for further investigation. To enable downstream follow-up for both
49 bacterial and mammalian genetic research communities, all bacterial fitness profiles
50 have been deposited into GeneNetwork.org and added into the comprehensive
51 collection of TnSeq libraries in MtbTnDB.
52
53 **Introduction**
54 Every pathogenic infection is part of an evolutionary battle between host and invader. In
55 the case of *Mycobacterium tuberculosis* (*Mtb*), the causative agent of tuberculosis (TB),
56 evidence tracing back at least 9,000 years tells the tale of a host-pathogen arms race
57 (Hershkovitz et al. 2008), making *Mtb* one of the most enduring adversaries of the
58 human species. Given the prevailing nature of this challenge, it is no surprise that
59 weaknesses in vital host defenses provide greater opportunity for *Mtb* infection,
60 allow *Mtb* to manipulate the nature and magnitude of the host immune response, and
61 worsen patient prognoses (Cooper et al. 1993; Flynn et al. 1993; Cooper et al. 1997;
62 Caruso et al. 1999; Kramnik et al. 2000). In addition, the advent of drug resistant and
63 multi-drug resistant *Mtb* strains highlights the imminent danger posed by our
64 microscopic rivals and underscores the importance of bacterial variation as a critical
65 factor in the pathogenesis and continued spread of *Mtb* (Caws et al. 2008; Hernández-
66 Pando et al. 2012; Gopal et al. 2014). Meanwhile, genetic diversity of both hosts and
67 *Mtb* strains that interact during infection can give rise to a spectrum of disease
68 outcomes (Smith and Sassetti 2018), enhancing the complexity of TB identification and
69 treatment. To combat a pathogen responsible for nearly 10.6 million infections and 1.6

70 million deaths annually (WHO 2022), it is therefore vital to dissect the host-pathogen
71 interface.
72
73 Mammalian models of TB have been used successfully to identify and mechanistically
74 interrogate TB susceptibility loci identified from human cohorts. For mouse strains that
75 are phenotypically divergent, quantitative trait locus (QTL) mapping studies within
76 genetically tractable and reproducible hosts have enabled the identification of genomic
77 loci that contribute to the magnitude of clinically relevant phenotypes (Lavebratt et al.
78 1999; Kramnik et al. 2000; Mitsos et al. 2000; Mitsos et al. 2003; Yan et al. 2006). The
79 classic inbred strains C57BL/6J (B6) and DBA/2J (D2) lie on opposite ends of the TB
80 susceptibility spectrum, with B6 surviving nearly a year post-infection and D2
81 succumbing to cachexia and morbidity within months (Medina and North 1998). To
82 capitalize on this diverse disease outcome and just over 6 million divergent SNPs
83 (Wang et al. 2016; Ashbrook et al. 2021; Ashbrook et al. 2022; Sasani et al. 2022), a
84 recombinant inbred panel generated from these two founders, known as the BXD, has
85 been used to understand host determinants of susceptibility to a variety of diseases
86 (Taylor et al. 1973; Taylor et al. 1999; Peirce et al. 2004; Ashbrook et al. 2021).
87
88 BXD and other recombinant inbred panels have been used to explore the intricate
89 dynamics of TB disease, but often the phenotypes leveraged to understand these
90 dynamics in mice, such as survival time post-infection, body weight, or bacterial burden,
91 are too complex and polygenic to reveal novel biology or enable refined mapping.
92 These “macrophenotypes” materialize from many genetic and environmental factors

that can be difficult to mechanistically dissect or precisely map. Within each unique host, bacteria face similarly diverse immunological dynamics and spatiotemporal selective pressures. To contribute to the growing body of work on genetic determinants of TB outcome, quantifying precise bacterial “endophenotypes” underlying disease outcomes is the crucial next step toward elaborating the biological intricacies that govern the host-pathogen interface. Recently employed molecular endophenotypes include expression QTL (Chesler et al. 2005), metabolite QTL (Wu et al. 2014), protein QTL (Chick et al. 2016), and chromatin accessibility QTL (Skelly et al. 2020), but for infectious disease, the most salient endophenotypes lie at the interface of the host and pathogen.

A classic approach to assess the requirement of a bacterial gene for infection is to infect a standard inbred mouse strain, such as B6, with a single knockout *Mtb* mutant. Expanding on this design, genome-wide mutagenesis enables the generation of single knockout mutants across the *Mtb* genome, thereby allowing the measurement of *Mtb* gene requirements under a variety of selective pressures. Transposon mutant libraries (TnSeq) have been successfully used to report on variable components of the bacterial infection microenvironment under distinct host and antibiotic pressures (Sassetti and Rubin 2003; Nambi et al. 2015; Mishra et al. 2017; Bellerose et al. 2019). We have recently leveraged TnSeq across genetically diverse Collaborative Cross (CC) mice to map both host- and pathogen-linked loci (Smith et al. 2022).

To further characterize the BXD phenome (Chesler et al. 2004) and add to the growing repertoire of selective pressures applied to *Mtb* whole-genome mutant libraries (Jinich et al. 2021), we now leverage the phenotypic divergence and reproducibility of the BXD family and the molecular phenotyping precision of an *Mtb* transposon mutant library. We infected parental genotypes and groups of mice from 19 BXD strains with a saturated library of *Mtb* transposon mutants and quantified mutant abundance within each host at one-month post infection. We conducted dual-genome QTL mapping to identify linkages between bacterial fitness profiles and host genetic factors, revealing 140 host genetic loci significantly associated with specific bacterial mutants. Thus, in passing a bacterial transposon mutant library through selection within the immunologically and phenotypically diverse BXD microenvironments, we have conducted a multidimensional host-pathogen screen to identify precise host and bacterial determinants of tuberculosis disease. Overall, this study provides a blueprint for the functional dissection of host-pathogen interactions that underlie diverse disease outcomes.

Materials & Methods

Ethics Statement

All mouse studies were conducted in accordance with the guidelines issued in the Guide for the Care and Use of Laboratory Animals of the National Institutes of Health and the Office of Laboratory Animal Welfare. Animal studies conducted at Duke University Medical School were conducted using protocols approved by the Duke Institutional Animal Care and Use Committee (IACUC) (Animal Welfare Assurance #A221-20-11) in a manner designed to minimize pain and suffering in *Mtb*-infected

138 animals. Any animal exhibiting signs of severe disease was immediately euthanized in
139 accordance with IACUC approved endpoints. All mouse studies conducted at the
140 University of Massachusetts Medical School (UMass) were performed using protocols
141 approved by UMass IACUC (Animal Welfare Assurance #A3306-01).
142
143 *Mice*
144 Male and female C57BL/6J (#000664) and DBA/2J (#000671) mice were purchased
145 from The Jackson Laboratory. Male mice from 19 BXD strains were imported from the
146 colony of Robert Williams (University of Tennessee Health Science Center, Memphis,
147 TN) in 2013. The 19 BXD strains in this study include: BXD9/TyJ, BXD29/Ty,
148 BXD39/TyJ, BXD40/ TyJ, BXD48a/RwwJ, BXD51/RwwJ, BXD54/RwwJ, BXD56/RwwJ,
149 BXD60/RwwJ, BXD62/RwwJ, BXD67/RwwJ, BXD69/RwwJ, BXD73/RwwJ,
150 BXD73b/RwwJ, BXD77/RwwJ, BXD79/RwwJ, BXD90/RwwJ, BXD93/RwwJ,
151 BXD102/RwwJ. All mice were housed in a specific pathogen-free facility within
152 standardized living conditions (12-hour light/dark, food and water *ad libitum*). Mice were
153 matched at 8-12 weeks of age at the time of *Mtb* infection. Male mice were used in the
154 TnSeq screen, and both male and female mice were used in the aerosol studies.
155
156 M. tuberculosis *Strains*
157 All *Mtb* strains were cultured in Middlebrook 7H9 medium supplemented with oleic acid-
158 albumin-dextrose catalase (OADC), 0.2% glycerol, and 0.05% Tween 80 to log-phase
159 with shaking (200 rpm) at 37˚C. Hygromycin (50 µg/mL) or kanamycin (20 µg/mL) were
160 added when necessary. Prior to all *in vivo* infections, cultures were washed,

resuspended in phosphate-buffered saline (PBS) containing 0.05% Tween 80 (hereafter PBS-T), and sonicated before diluting to desired concentration.

Mouse Infections

For aerosol infections, B6 and D2 were infected with ~50 colony forming units (CFU) of *Mtb* H37Rv YFP via aerosol inhalation (Glas-Col) for 6 and 12 weeks. At each timepoint, male and female mice were euthanized in accordance with approved IACUC protocols, and lung and spleen were harvested into PBS-T and homogenized. CFU was quantified by dilution plating onto Middlebrook 7H10 agar supplemented with OADC, 0.2% glycerol, 50 mg/mL Carbenicillin, 10 mg/mL Amphotericin B, 25 mg/mL Polymixin B, and 20 mg/mL Trimethoprim. One lung lobe per mouse was collected into 10% neutral-buffered formalin for H&E staining by the Duke University Research Immunohistology Laboratory.

For TnSeq experiments, $1x10^6$ CFU of saturated *Himar1* transposon mutants (Sassetti et al. 2003) was delivered via intravenous tail vein injection. Mice were infected in a single batch. At 4 weeks post-infection, mice were euthanized, and spleens and lungs were harvested then homogenized in a FastPrep-24 (MP Biomedicals). CFU was quantified by dilution plating on 7H10 agar with 20 µg/mL Kanamycin. For library recovery, approximately $1x10^6$ CFU per mouse was plated on 7H10 agar with 20 µg/mL Kanamycin. After three weeks of growth, colonies were harvested by scraping, and genomic DNA was extracted. The relative abundance of each transposon mutant was estimated as described in Long et al. 2015.

184

185 *Microscopy and Damage Quantification*

186 H&E-stained lung sections were imaged in bright field at 2X magnification on the
187 Keyence BZ-X800. Images were processed identically within FIJI software
188 (v2.3.0/1.53p) for image clarity. To quantify damage, an artificial neural network-based
189 damage identification model was developed within QuPath (v0.3.2). Eight images (1
190 image per experimental group) were utilized for the single purpose of training the model,
191 and the remaining 3 images per group were quantified using the model. To prevent
192 bias, lung sections presented in this report were quantified as the closest to the mean
193 damage of each experimental group.

194

195 *TnSeq Analysis*

196 TnSeq libraries were prepared and transposon insertion counts were estimated as
197 previously described (Smith et al. 2022). The H37Rv genome annotation used is NCBI
198 Reference Sequence NC_018143.2. In total, 40 independent transposon libraries were
199 sequenced after recovery from the 19 BXD genotypes and the two parent strains, B6
200 and D2. Two independent transposon libraries were placed under selection within each
201 host genotype. However, in the cases of two BXD genotypes, BXD48a and BXD51, only
202 one library could be sufficiently recovered for sequencing. Within TRANSIT (DeJesus et
203 al. 2015), beta-geometric correction was used to normalize insertion mutant counts
204 across all libraries, and pseudocounts were implemented. Insertion counts were totaled
205 for each *Mtb* gene, and counts were averaged between individual replicate libraries per
206 mouse. Per gene mean values were compared to the grand mean then $\log_2$

transformed.

To control for multiple hypotheses genome-wide, 10,000 permutation tests were performed to generate a resampling distribution used to derive the significance of transposon mutant selection between *in vitro* and *in vivo* conditions. An *Mtb* gene was considered "essential" within a host if mutants lacking that gene experienced a $\log_2$ fold change (LFC) value of -0.5 or lower post-selection in that host. To identify *Mtb* genes whose fitness was sufficiently variable to enable QTL mapping, the dynamic range in LFC across the parental and BXD strains for any given bacterial gene had to be at least 0.63. This value is the minimum LFC range of a mutant that was significantly selected in at least one host genotype after resampling ($Q < 0.05$). Mutants used for QTL mapping also needed to be sufficiently represented in the library, which was accomplished by requiring 4 or more TA transposon insertion sites to be detected for each bacterial gene. Further, each gene included needed to be significantly selected in at least one host genotype before resampling ($p < 0.05$).

Genotyping and QTL Mapping

Previously published BXD genotypes containing 7,321 total markers were leveraged for QTL mapping (Wang et al. 2016). Markers that were not diagnostic of genetic differences between B6 and D2 were filtered out resulting in a total of 7,314 markers. Genotype data and phenotype data, including lung and spleen burden and TnSeq mutant fitness profiles, were imported into R statistical software (version 4.1.1) and formatted for QTL mapping within R/qtl2 (version 0.28) (Broman et al. 2019). The Leave

One Chromosome Out (LOCO) approach was leveraged to estimate kinship between strains as a covariate for QTL mapping. Because all screened mice were male and infected in one batch, no other covariates were used for the initial mapping. Logarithm of odds (LOD) scores were calculated using the linear mixed model in R/qtl2 to establish phenotypic associations with marker loci across the host genome. Trait-wise significance thresholds for QTL were established by 10,000 permutation tests. The significance of gene class overrepresentation among the mapped QTL in comparison to class representation in the whole *Mtb* genome was established using Fisher's Exact Test.

Results

B6 and D2 mouse strains experience distinct chronic disease profiles after aerosol infection

B6 and D2, the parent strains of the BXD panel, have divergent responses to *Mtb* infection (Chackerian and Behar 2003). Canonically considered *Mtb*-resistant, the T_H1-skewed adaptive immune response initiated by B6 mice is capable of restraining *Mtb* growth after ~21 days, resulting in a mean survival time of ~230 days (Mitsos et al. 2000). However, D2 mice experience low IFN-γ-producing T cell influx to the lung at 21 days, when adaptive immunity should begin, at which point B6 and D2 begin to diverge in bacterial growth restriction (**Figure 1A & B**) and lung damage (**Figure 1C**-**E**) (Marquis et al. 2008). D2 macrophages become foamy and dysfunctional, making it difficult to contain and control bacterial growth in the lung (Chackerian and Behar 2003). By 12 weeks post-aerosol infection, D2 lungs exhibit

hyperinflammatory and fibrotic responses leading to overt damage (**Figure 1F**-**H**) and an ultimate mean survival time of ~110 days (Medina and North 1998; Keller et al. 2006). In addition to genotype-specific differences between these BXD parent strains, we also observe a sex effect independent of genotype, demonstrated by higher susceptibility of males of both genotypes (**Figure S1A & B**) (Tsuyuguchi et al. 2001; Dibbern et al. 2017). Further, we find that in contrast to burden, all groups reduce lung damage by week 12 except for D2 males (**Figure S1C**-**G**).

Early clinical macrophenotypes fail to distinguish parental disease outcomes

With over 100 still extant recombinant inbred strains bred from B6 and D2 parental strains, the BXD family is a well-suited mammalian resource to map the phenotypic diversion during *Mtb* infection (**Figure 2A**). To study early disease traits and bacterial endophenotypes that predict differences in TB disease outcomes during chronic infection stages, we intravenously infected cohorts of the parental B6 and D2 lines and 19 BXD genotypes with a saturated TnSeq library of transposon (Tn) mutants. The Tn library contains knockouts of every *Mtb* gene that is not required *in vitro*, which collectively produces an infection similar to the wildtype infection strain (Sassetti and Rubin 2003; Smith et al. 2022). At 4 weeks post-infection, the parental B6 and D2 strains demonstrated approximately the same bacterial burden in lung and spleen (**Figure 2B**). Moreover, BXD strains did not exhibit sufficiently wide variation in bacterial burden at 4 weeks post-infection to precisely map the genetic cause of such a complex trait (**Figure 2C**; **Figure S2A** & **B**). Compound macrophenotypes, such as colony forming units (CFU) in organ homogenate, are highly polygenic, making it difficult to

identify causal genes even with large panels of mice (Lavebratt et al. 1999; Mitsos et al. 2000; Mitsos et al. 2003; Yan et al. 2006).

Transposon mutant fitness endophenotypes report on the host immunological microenvironment

To interrogate the biological mechanisms that predict immunodivergent outcomes, we quantified the abundance of each bacterial Tn mutant both before host infection with the TnSeq library and after recovery from mouse organs of each genotype. The $\log_2$ fold change (LFC) of abundance was calculated as a quantification of relative mutant fitness in each host condition. This LFC fitness value serves as a precise reporter of the host microenvironment and can be used to map host loci that impact *Mtb* mutant fitness (**Figure 3A**).

Across the BXD panel, we identified three main classes of bacterial mutants, which are highlighted in **Figure 3B**. The first of these classes includes canonical *Mtb* genes that are essential for *in vivo* survival, exemplified by *bioA*. These genes remain essential for *Mtb* survival in both parental backgrounds and across the BXD strains (**Figure 3B**; "essential" profile in red). A second, "differentially required" set of mutants is exemplified in this figure by *mbtG*; the loss of *mbtG* did not significantly reduce bacterial fitness within B6 mice, but *mbtG* mutants experienced an extreme fitness reduction within D2 mice (**Figure 3B**; "differentially required" profile in yellow). Further, there is a spectrum of *mbtG* essentiality across the family, indicating that some variable host factor could modify the fitness of this mutant. In addition to *in vivo* essential and differentially

299 essential *Mtb* genes, a third class of *Mtb* genes proved to be broadly dispensable
300 for *Mtb* survival in these hosts, imparting an adaptive benefit for *Mtb* when the gene was
301 disturbed, represented here by *glpK* (**Figure 3B**; “non-essential” profile in green).
302
303 When surveying the complete set of *Mtb* transposon mutants, we find that in
304 comparison with B6 infection, *Mtb* requires almost twice as many genes to survive
305 within D2 mice (**Figure 3C**). This finding suggests that there are detectable
306 immunological pressures being exerted on *Mtb* within the highly inflammatory D2 line
307 prior to the divergence in B6 and D2 bacterial control and disease outcome. This result
308 replicates findings from previous work in which a greater number of *Mtb* genes were
309 essential in T cell-deficient and IFN-γ-deficient mice than in B6 (Mishra et al. 2017;
310 Smith et al. 2022). We additionally find that the BXD panel, while recapitulating most
311 B6- and D2-essential genes, reveals additional subsets of genes that are only required
312 within specific BXD strains (**Figure 3D**), highlighting the power of this genetically
313 diverse panel to offer novel insights into the biology controlling TB outcome.
314
315 This spectrum of *Mtb* gene essentiality is further confirmed when we examine the
316 correlation of the complete TnSeq library fitness between hosts (**Figure 3E**).
317 Interestingly, the majority of the strains hierarchically clustered closer to D2 than to B6,
318 indicating that they could be inheriting factors from D2 that put greater immunological
319 pressure on *Mtb*.
320

Transposon mutant fitness profiles map host-pathogen *QTL (*hp*QTL)*

We aimed to use these bacterial mutants as sensitive reporters of host immunological pressures within the early phase of infection at the onset of adaptive immunity. Using the LFC values collected for each Tn mutant population in the TnSeq library as quantitative endophenotypes (**Table S1**), we conducted QTL mapping. After removing non-dynamic genes for quality control (**Figure S3A**; *Mtb* genes that are not sufficiently varying in essentiality across the screened BXD genotypes), we found 140 genome-wide significant QTL, defined as $p \leq 0.05$ after 10,000 permutations (**Table 1**). Of these QTL, 33 of the loci had a p-value ≤ 0.01 (**Figure 4A**).

Among the most significant QTL mapped in the screen, certain gene classes were marginally overrepresented in comparison to the genome-wide abundance of that class. Transposon mutants lacking genes that encode known virulence factors made up 12.1% of the top hits in this screen despite only representing 5.8% of the *Mtb* genome ($p = 0.1$) (**Figure 4B**) (Kapopoulou et al. 2011). Further, lipid metabolism genes made up 15.2% of the bacterial mutants mapping highly significant QTL while representing 6.6% of the *Mtb* genome ($p = 0.07$). Certain gene classes were abundant in approximately equal proportions in the mapped QTL as they were genome-wide, such as metabolism and respiration genes (22.8% among top QTL vs. 24.2% genome-wide prevalence) and genes encoding PPE/PE proteins (3.0% among top QTL vs. 4.1% genome-wide prevalence). Roughly half of *Mtb* protein coding genes remain unannotated (Whitaker et al. 2020), and 7 of the highly significant ($p \leq 0.01$) bacterial fitness traits mapped by this screen correspond to bacterial genes with no known

function. Taking these screen data in combination with previous *in vivo* TnSeq studies, these data will contribute to the de-orphanization of much of the *Mtb* genome.

Multiple highly significant QTL map to host chromosome 6 "hotspot"

The nature of this screen enabled the discovery of host loci that impact the fitness of numerous bacterial mutants. Among the QTL mapped in this screen, 5 QTL mapped to chromosome 7 (**Figure 4A**), yet the 95% confidence intervals for each QTL span such a large part of the chromosome that identifying a causal host gene would be infeasible without further experimentation. Aside from the chromosome 7 locus, there appears to be a much narrower region on chromosome 6 (75.97–88.58 Mb) strongly linked to the essentiality of four bacterial genes: *Rv0127* (*mak;* sometimes annotated as *pep2*), *Rv0359* (*rip2*), *Rv0955* (*perM*), *Rv3849* (*espR*) (**Figure 5A-E**). For each of the mutants lacking these bacterial genes, apart from *perM*, the B6 sequence in this region is associated with lower bacterial mutant fitness (**Figure 5F-I**; **Figure S4A-E**). *Mtb* mutants lacking *perM* experience a fitness cost within genotypes that possess the *D* haplotype in this region.

This QTL hotspot is mapped by *Mtb* genes that impact metabolism, virulence, and defense. Mak catalyzes the ATP-dependent conversion of maltose into maltose-1-phosphate as a part of the glycogen biosynthesis pathway that supports construction of the protective outer capsule of *Mtb* (Li et al. 2014). Of note, TreS, which converts trehalose to maltose upstream of Mak, also maps to a genome-wide significant QTL on chromosome 11 and has done so in previous *Mtb* infection screens (Smith et al. 2022).

rip2 is a putative zinc metalloprotease located in the *Mtb* cell membrane (Sklar et al. 2010), although very little is known about its function. PerM is an integral membrane protein that is known to play an essential role in enabling bacterial cell division under acid stress in B6 mice (Wang et al. 2019). Here, we report that *perM* mutants are even more severely attenuated within a D2 background, implying that PerM is differentially impacted by host immunological pressures. EspR is a key regulator of the ESX-1 secretion system (Rosenberg et al. 2011; Blasco et al. 2012), which itself plays a well-established role in mycobacterial virulence. Mutants lacking these bacterial genes map significant QTL within the interval of 75.97–88.58 Mb on mouse chromosome 6.

The 95% Bayesian confidence intervals of the QTL mapped by *rip2* and *perM* mutants overlap while the confidence intervals of *mak* and *espR* mutants overlap separately from the *rip2* and *perM* QTL. To test for the independence of these two groups of nearby QTL, we re-mapped each of the QTL within the chromosome 6 hotspot, iteratively incorporating the haplotype possessed by each BXD strain at each QTL as an additive covariate. Dependent loci will not map if the haplotype of one locus is factored into the mapping pipeline as a covariate. Conversely, the ability of a QTL to achieve significance independent of the haplotype state at another locus suggests that the two loci arise from distinct causal genetic factors within the host. These tests suggested two causal host loci exist within this highly significant QTL hotspot: one host factor underlying the *rip2* and *perM* mutant fitness QTL and one underlying the *mak* and *espR* QTL (**Figure 6A-D**).

To identify host gene candidates that may mediate the survival of these two groups of bacterial mutants, we defined a pipeline to select for protein coding genes for which *D* haplotype has a unique SNP in comparison to *B* haplotype (**Figure 7A**). We passed each of the genes identified by this pipeline through a list of genetic and clinical criteria using independent but complementary data sets from a variety of *Mtb*-infected mammalian cohorts (**Figure 7B**) (Zak et al. 2016; Moreira-Teixeira et al. 2017; Ahmed et al. 2020). From this comparative analysis, we identified a putative host candidate within the region mapped by *mak*: MAX dimerization protein 1 (*Mxd1*), which is known to be upregulated in murine bone marrow-derived macrophages after infection with the hypervirulent *Mtb* HN878 strain (Roy et al. 2018). Further, we found a putative host candidate within the QTL mapped by *perM* mutants: ancient ubiquitous protein 1 (*Aup1*). Altogether, we have leveraged complementary screen data to identify plausible host gene candidates underlying these host-pathogen QTL.

Discussion

While it is thought that nearly a quarter of the global population is infected with *Mtb* (Houben and Dodd 2016), only 5–10% of *Mtb* infections ultimately result in active TB (Gopal et al. 2014). This paradox has motivated decades of study on human genetic variants that could predict such a lethal prognosis in affected individuals. While GWAS among infected populations has identified numerous host loci associated with increased susceptibility to disease, a limited ability to dissect biological mechanism leaves many questions unanswered (Saul et al. 2019). QTL mapping, a parallel systems genetics

technique, has been utilized for decades to identify host loci in genetically tractable populations linked to TB susceptibility; *Sst1* (susceptibility to tuberculosis 1), one of the most well-known TB susceptibility loci, was first discovered through a QTL mapping study in mice (Kramnik et al. 2000). Despite the widespread use of disease traits, including mean survival time, body weight, and bacterial burden, to identify host determinants of disease progression (Lavebratt et al. 1999; Kramnik et al. 2000; Mitsos et al. 2000; Mitsos et al. 2003; Yan et al. 2006), these phenotypes can be challenging to dissect immunological features that drive distinct *Mtb* pathogenesis in diverse hosts. Here, we describe a screen in which we leveraged the reproducibility, host variation, and phenotypic divergence of the BXD family and the molecular precision of the TnSeq library to identify novel axes of host-pathogen interaction during *Mtb* infection. We demonstrate the late (12 week) phenodivergence of the parental B6 and D2 mice, however we found that CFU serves as a weak predictor of host outcome at the onset of adaptive immunity 4 weeks post-infection. By utilizing TnSeq as a refined infection trait, we identified bacterial mutants that could distinguish the resistant B6 and susceptible D2 strains at the early 4 weeks infection timepoint. Finally, we leveraged the differentially required mutants as traits to conduct QTL mapping and identified 140 genome-wide *hp*QTL and a QTL hotspot encompassing a cluster of *Mtb* virulence and cell wall genes. Using this BXD TnSeq platform and a novel candidate prioritization pipeline, we identified viable host gene candidates for future study.

This screen highlights the importance of intentionality in design for deep phenotyping platforms to optimally identify the causal factors underlying gene associations. In

436 contrast to complex macrophenotypes, which require hundreds of mice to sufficiently
437 power causal locus identification for highly polygenic traits, molecular endophenotypes,
438 such as *Mtb* transposon mutant fitness, allow us to learn more about the intricate details
439 of *Mtb* invasion in the early stages of infection, which is particularly helpful in an
440 experimental framework with fewer host genotypes. The strength of TnSeq as a deep
441 phenotyping platform lies in the redundancy of each *Mtb* gene knockout; within the
442 TnSeq library, each bacterial gene that is non-essential *in vitro* was perturbed at 4 or
443 more unique transposon insertion sites, resulting in multiple subpopulations of unique
444 replicates of each *Mtb* gene knockout. These mutant replicates taken together paint a
445 robust picture of individual *Mtb* gene requirement *in vivo*, and multiple host replicates
446 strengthen the reproducibility of each *Mtb* mutant fitness profile. In contrast with our
447 previous TnSeq study that utilized nearly 70 host genotypes (Smith et al. 2022), this
448 TnSeq study includes 21 unique genotypes and 73 mice, including the parental strains
449 B6 and D2. The greater number of transposon mutant *hp*QTL identified in this screen
450 demonstrates the power of a two-state model to segregate allele effects, as opposed to
451 the eight-state model present in the Collaborative Cross recombinant inbred panel. We,
452 however, cannot eliminate the possibility that the smaller number of host genotypes
453 included in this study did not sufficiently limit statistical noise during QTL mapping
454 analyses.
455
456 Using bacterial mutant profiles as endophenotypes, we identified 140 genome-wide
457 significant ($p \leq 0.05$) associations between *Mtb* transposon mutant survival and host
458 genetic loci in a diverse cohort, which may contribute to divergence in clinical outcomes

between *Mtb*-resistant and susceptible hosts. These host-pathogen QTL (*hp*QTL) and the transposon mutant fitness profiles across the BXD panel have been shared with GeneNetwork.org (Chesler et al. 2004; Parker et al. 2017; Ashbrook et al. 2021), an online compendium of BXD phenotypes. Increasing the precision of bacterial traits creates a rich environment for screen-based hypothesis generation in a smaller host population, thereby lowering the cost through lower animal count and less total infection time. This screen serves as a proof-of-concept that large host populations are not an absolute necessity to uncover novel and biologically meaningful axes of the host-pathogen interface. Molecular endophenotyping enables a much more accessible experimental platform to assist in our ongoing struggle against *Mtb*.

From this discovery screen, we have identified several plausible host gene candidates. Variants in *Aup1* represent a possible axis for interaction between *Mtb* and the mammalian host. The acetyltransferase activity of *Aup1* has been shown to be exploited by flaviviruses to trigger autophagy of lipid droplets within the cell, which produces ATP for the virus, thereby promoting viral replication (Zhang et al. 2018). Although not much is known about whether *Mtb* interacts directly with this protein, *Mtb* is one of the few bacteria capable of generating lipid droplets (Daniel et al. 2011). Host lipid droplets, specifically those derived from foamy macrophages, have been shown to promote the production of defensive cytokines during *Mtb* infection (Jaisinghani et al. 2018), implicating a potentially intriguing locus for host-pathogen interaction. The other high priority candidate *Mxd1* encodes the protein MAD, which competes with MYC to bind with MAX, forming a transcriptional repressor. This mechanism has led *Mxd1* to be

482 considered a putative tumor suppressor gene. *Mxd1* has been shown to be upregulated
483 in murine bone marrow-derived macrophages upon initial infection with the hypervirulent
484 *Mtb* HN878 strain (Roy et al. 2018) and to regulate the fitness of murine dendritic cells
485 (Anderson et al. 2020), yet the function of *Mxd1* in response to *Mtb* has yet to be
486 determined. Together these candidates provide feasible next steps for mechanistic
487 interrogation of these loci.
488
489 While the functions of many mycobacterial genes remain unknown (Whitaker et al.
490 2020), this transposon mutant screen within the BXD family builds directly upon a
491 previous screen in the Collaborative Cross panel (Smith et al. 2022) to further articulate
492 the conditional necessity of many canonically “non-essential” *Mtb* genes within a
493 spectrum of host microenvironments. A substantial number of *Mtb* genes known to be
494 non-essential in B6 mice prove to be essential in a subset of these genetically diverse
495 hosts, suggesting that these bacterial genes play an active yet undiscovered role in
496 pathogenesis under specific immunological conditions. These new host conditions have
497 been shared with MtbTnDB (Jinich et al. 2021), a central repository encompassing over
498 60 published *Mtb* TnSeq screens for ease of browsing and inter-screen comparison. For
499 mycobacterial researchers exploring *Mtb* genes traditionally thought to be non-essential
500 *in vivo*, this work challenges such a notion and offers a new model that will provide
501 insight into the host-pathogen dynamic underlying this conditional *in vivo* essentiality.
502
503 **Data Availability Statement**
504 All relevant data to support the findings of this study are located within the paper and

supplementary files. Genome sequence data is being deposited in the NCBI Gene Expression Omnibus (GEO). Transposon mutant fitness profiles within each BXD genotype and parental genotypes will be made publicly available on MtbTnDB (https://www.mtbtndb.app/). BXD phenotypes are available on GeneNetwork (https://www.genenetwork.org).

Acknowledgements

We thank Anna Tyler, Matthew Mahoney, and Greg Carter for their assistance in concept development; Emily Hunt, Kris Riebe, and Summer Harris for technical assistance; Erin Curtis for graphic design and thoughtful discussions; Tobin and Smith Lab members for constructive feedback; Arthur Centeno for BXD phenotype import to WebQTL; and Douglas Marchuk for insightful comments on the manuscript. We are especially grateful to Richard Baker for rigorous biostatistical suggestions, meticulous data management and analysis, and conceptual development. Biocontainment work was partially performed in the Duke Regional Biocontainment Laboratory, which received partial support for construction from the National Institutes of Health, National Institute of Allergy and Infectious Diseases (UC6-AI058607; G20-AI167200).

Funder Information

This work was funded by a Whitehead Scholar Award and an NIH Director's New Innovator Award (1DP2-GM146458) to C.M.Smith; AI132130 to C.M.Sassetti; AI162584 to K.Y.R; R01GM123489 to R.W.W.

Conflict of Interest

The authors declare no conflicts of interest.

Literature Cited

Adams DJ, Doran AG, Lilue J, Keane TM. 2015. The Mouse Genomes Project: a repository of inbred laboratory mouse strain genomes. Mamm Genome 2015 269. 26(9):403–412. doi:10.1007/S00335-015-9579-6. [accessed 2022 Sep 26]. https://link.springer.com/article/10.1007/s00335-015-9579-6.

Ahmed M, Thirunavukkarasu S, Rosa BA, Thomas KA, Das S, Rangel-Moreno J, Lu L, Mehra S, Mbandi SK, Thackray LB, et al. 2020. Immune correlates of tuberculosis disease and risk translate across species. Sci Transl Med. 12(528). doi:10.1126/scitranslmed.aay0233. [accessed 2020 Sep 12]. https://stm.sciencemag.org/content/12/528/eaay0233.

Anderson DA, Murphy TL, Eisenman RN, Murphy KM. 2020. The MYCL and MXD1 transcription factors regulate the fitness of murine dendritic cells. Proc Natl Acad Sci U S A. 117(9):4885–4893. doi:10.1073/PNAS.1915060117/SUPPL_FILE/PNAS.1915060117.SAPP.PDF. [accessed 2022 May 9]. www.pnas.org/cgi/doi/10.1073/pnas.1915060117.

Ashbrook DG, Arends D, Prins P, Mulligan MK, Roy S, Williams EG, Lutz CM, Valenzuela A, Bohl CJ, Ingels JF, et al. 2021. A platform for experimental precision medicine: The extended BXD mouse family. Cell Syst. 12(3):235-247.e9. doi:10.1016/J.CELS.2020.12.002/ATTACHMENT/F0DA3833-3075-4DFD-8329-60E18E7E4749/MMC5.XLSX. [accessed 2022 Oct 21].

http://www.cell.com/article/S2405471220305032/fulltext.

Ashbrook DG, Sasani T, Maksimov M, Gunturkun MH, Ma N, Villani F, Ren Y, Rothschild D, Chen H, Lu L, et al. 2022. Private and sub-family specific mutations of founder haplotypes in the BXD family reveal phenotypic consequences relevant to health and disease. bioRxiv.:2022.04.21.489063. doi:10.1101/2022.04.21.489063. [accessed 2023 Mar 1]. https://www.biorxiv.org/content/10.1101/2022.04.21.489063v1.

Bellerose MM, Baek SH, Huang CC, Moss CE, Koh EI, Proulx MK, Smith CM, Baker RE, Lee JS, Eum S, et al. 2019. Common variants in the glycerol kinase gene reduce tuberculosis drug efficacy. MBio. 10(4). doi:10.1128/MBIO.00663-19/ASSET/D1B2922E-7867-4292-8B92-199E749000E9/ASSETS/GRAPHIC/MBIO.00663-19-F0005.JPEG. [accessed 2022 Mar 24]. https://journals.asm.org/doi/full/10.1128/mBio.00663-19.

Blasco B, Chen JM, Hartkoorn R, Sala C, Uplekar S, Rougemont J, Pojer F, Cole ST. 2012. Virulence Regulator EspR of Mycobacterium tuberculosis Is a Nucleoid-Associated Protein. PLOS Pathog. 8(3):e1002621. doi:10.1371/JOURNAL.PPAT.1002621. [accessed 2022 May 9]. https://journals.plos.org/plospathogens/article?id=10.1371/journal.ppat.1002621.

Broman KW, Gatti DM, Simecek P, Furlotte NA, Prins P, Sen Ś, Yandell BS, Churchill GA. 2019. R/qtl2: Software for mapping quantitative trait loci with high-dimensional data and multiparent populations. Genetics. 211(2):495–502. doi:10.1534/genetics.118.301595. [accessed 2020 Sep 8]. https://doi.org/10.1534/genetics.118.301595.

574 Caruso AM, Serbina N, Klein E, Triebold K, Bloom BR, Flynn JL. 1999. Mice Deficient in
575 CD4 T Cells Have Only Transiently Diminished Levels of IFN-γ, Yet Succumb to
576 Tuberculosis. J Immunol. 162(9):5407–5416. doi:10.4049/jimmunol.162.9.5407.
577 [accessed 2023 Feb 10]. https://pubmed.ncbi.nlm.nih.gov/10228018/.
578 Caws M, Thwaites G, Dunstan S, Hawn TR, Lan NTN, Thuong NTT, Stepniewska K,
579 Huyen MNT, Nguyen DB, Tran HL, et al. 2008. The Influence of Host and Bacterial
580 Genotype on the Development of Disseminated Disease with Mycobacterium
581 tuberculosis. PLOS Pathog. 4(3):e1000034. doi:10.1371/JOURNAL.PPAT.1000034.
582 [accessed 2022 Mar 24].
583 https://journals.plos.org/plospathogens/article?id=10.1371/journal.ppat.1000034.
584 Chackerian AA, Behar SM. 2003. Susceptibility to Mycobacterium tuberculosis: Lessons
585 from inbred strains of mice. Tuberculosis. 83(5):279–285. doi:10.1016/S1472-
586 9792(03)00017-9.
587 Chesler EJ, Lu L, Shou S, Qu Y, Gu J, Wang J, Hsu HC, Mountz JD, Baldwin NE,
588 Langston MA, et al. 2005. Complex trait analysis of gene expression uncovers
589 polygenic and pleiotropic networks that modulate nervous system function. Nat
590 Genet 2005 373. 37(3):233–242. doi:10.1038/ng1518. [accessed 2022 Mar 24].
591 https://www.nature.com/articles/ng1518.
592 Chesler EJ, Lu L, Wang J, Williams RW, Manly KF. 2004. WebQTL: rapid exploratory
593 analysis of gene expression and genetic networks for brain and behavior. Nat
594 Neurosci 2004 75. 7(5):485–486. doi:10.1038/nn0504-485. [accessed 2022 Mar 24].
595 https://www.nature.com/articles/nn0504-485.
596 Chick JM, Munger SC, Simecek P, Huttlin EL, Choi K, Gatti DM, Raghupathy N,

597 Svenson KL, Churchill GA, Gygi SP. 2016. Defining the consequences of genetic
598 variation on a proteome-wide scale. Nat 2016 5347608. 534(7608):500–505.
599 doi:10.1038/nature18270. [accessed 2022 Mar 24].
600 https://www.nature.com/articles/nature18270.
601 Cooper AM, Dalton DK, Stewart TA, Griffin JP, Russell DG, Orme IM. 1993.
602 Disseminated tuberculosis in interferon gamma gene-disrupted mice. J Exp Med.
603 178(6):2243–2247. doi:10.1084/JEM.178.6.2243. [accessed 2023 Feb 10].
604 https://pubmed.ncbi.nlm.nih.gov/8245795/.
605 Cooper AM, Magram J, Ferrante J, Orme IM. 1997. Interleukin 12 (IL-12) is crucial to
606 the development of protective immunity in mice intravenously infected with
607 mycobacterium tuberculosis. J Exp Med. 186(1):39–45. doi:10.1084/JEM.186.1.39.
608 [accessed 2023 Feb 10]. https://pubmed.ncbi.nlm.nih.gov/9206995/.
609 Daniel J, Maamar H, Deb C, Sirakova TD, Kolattukudy PE. 2011. Mycobacterium
610 tuberculosis Uses Host Triacylglycerol to Accumulate Lipid Droplets and Acquires a
611 Dormancy-Like Phenotype in Lipid-Loaded Macrophages. PLOS Pathog.
612 7(6):e1002093. doi:10.1371/JOURNAL.PPAT.1002093. [accessed 2022 May 9].
613 https://journals.plos.org/plospathogens/article?id=10.1371/journal.ppat.1002093.
614 DeJesus MA, Ambadipudi C, Baker R, Sassetti C, Ioerger TR. 2015. TRANSIT - A
615 Software Tool for Himar1 TnSeq Analysis. PLOS Comput Biol. 11(10):e1004401.
616 doi:10.1371/JOURNAL.PCBI.1004401. [accessed 2022 May 9].
617 https://journals.plos.org/ploscompbiol/article?id=10.1371/journal.pcbi.1004401.
618 Dibbern J, Eggers L, Schneider BE. 2017. Sex differences in the C57BL/6 model of
619 Mycobacterium tuberculosis infection. Sci Rep. 7(1). doi:10.1038/s41598-017-11438-

z. [accessed 2020 Nov 11]. https://pubmed.ncbi.nlm.nih.gov/28887521/.

Flynn JAL, Chan J, Triebold KJ, Dalton DK, Stewart TA, Bloom BR. 1993. An essential role for interferon γ in resistance to mycobacterium tuberculosis infection. J Exp Med. 178(6):2249–2254. doi:10.1084/jem.178.6.2249.

Gopal R, Monin L, Slight S, Uche U, Blanchard E, A. Fallert Junecko B, Ramos-Payan R, Stallings CL, Reinhart TA, Kolls JK, et al. 2014. Unexpected Role for IL-17 in Protective Immunity against Hypervirulent Mycobacterium tuberculosis HN878 Infection. Lewinsohn DM, editor. PLoS Pathog. 10(5):e1004099. doi:10.1371/journal.ppat.1004099. [accessed 2021 Mar 16]. https://dx.plos.org/10.1371/journal.ppat.1004099.

Hernández-Pando R, Marquina-Castillo B, Barrios-Payán J, Mata-Espinosa D. 2012. Use of mouse models to study the variability in virulence associated with specific genotypic lineages of Mycobacterium tuberculosis. Infect Genet Evol. 12(4):725–731. doi:10.1016/j.meegid.2012.02.013.

Hershkovitz I, Donoghue HD, Minnikin DE, Besra GS, Lee OY-C, Gernaey AM, Galili E, Eshed V, Greenblatt CL, Lemma E, et al. 2008. Detection and Molecular Characterization of 9000-Year-Old Mycobacterium tuberculosis from a Neolithic Settlement in the Eastern Mediterranean. Ahmed N, editor. PLoS One. 3(10):e3426. doi:10.1371/journal.pone.0003426. [accessed 2020 Sep 5]. https://dx.plos.org/10.1371/journal.pone.0003426.

Houben RMGJ, Dodd PJ. 2016. The Global Burden of Latent Tuberculosis Infection: A Re-estimation Using Mathematical Modelling. Metcalfe JZ, editor. PLOS Med. 13(10):e1002152. doi:10.1371/journal.pmed.1002152. [accessed 2021 Mar 16].

643 https://dx.plos.org/10.1371/journal.pmed.1002152.

644 Jaisinghani N, Dawa S, Singh K, Nandy A, Menon D, Bhandari PD, Khare G, Tyagi A,
645 Gandotra S. 2018. Necrosis driven triglyceride synthesis primes macrophages for
646 inflammation during Mycobacterium tuberculosis infection. Front Immunol.
647 9(JUL):1490. doi:10.3389/FIMMU.2018.01490/BIBTEX.

648 Jinich A, Zaveri A, DeJesus MA, Flores-Bautista E, Smith CM, Sassetti F CM, Rock C
649 JM, Ehrt S, Schnappinger D, Ioerger G TR, et al. 2021. The Mycobacterium
650 tuberculosis transposon sequencing database (MtbTnDB): a large-scale guide to
651 genetic conditional essentiality. doi:10.1101/2021.03.05.434127. [accessed 2022
652 Mar 24]. https://doi.org/10.1101/2021.03.05.434127.

653 Kapopoulou A, Lew JM, Cole ST. 2011. The MycoBrowser portal: A comprehensive and
654 manually annotated resource for mycobacterial genomes. Tuberculosis. 91:8–13.
655 doi:10.1016/j.tube.2010.09.006. [accessed 2022 Aug 30]. http://pfam.sanger.ac.uk/.

656 Keller C, Hoffmann R, Lang R, Brandau S, Hermann C, Ehlers S. 2006. Genetically
657 determined susceptibility to tuberculosis in mice causally involves accelerated and
658 enhanced recruitment of granulocytes. Infect Immun. 74(7):4295–4309.
659 doi:10.1128/IAI.00057-06. [accessed 2020 Aug 11].
660 /pmc/articles/PMC1489748/?report=abstract.

661 Kramnik I, Dietrich WF, Demant P, Bloom BR. 2000. Genetic control of resistance to
662 experimental infection with virulent Mycobacterium tuberculosis. Proc Natl Acad Sci
663 U S A. 97(15):8560–8565. doi:10.1073/pnas.150227197. [accessed 2020 Aug 14].
664 /pmc/articles/PMC26987/?report=abstract.

665 Lavebratt C, Apt AS, Nikonenko B V., Schalling M, Schurr E. 1999. Severity of

Tuberculosis in Mice is Linked to Distal Chromosome 3 and Proximal Chromosome 9. J Infect Dis. 180(1):150–155. doi:10.1086/314843. [accessed 2022 Mar 24]. https://academic.oup.com/jid/article/180/1/150/990315.

Li J, Guan X, Shaw N, Chen W, Dong Y, Xu X, Li X, Rao Z. 2014. Homotypic dimerization of a maltose kinase for molecular scaffolding. Sci Rep. 4. doi:10.1038/SREP06418. [accessed 2022 May 9]. /pmc/articles/PMC4171701/.

Long JE, Dejesus M, Ward D, Baker RE, Ioerger T, Sassetti CM. 2015. Identifying essential genes in mycobacterium tuberculosis by global phenotypic profiling. Methods Mol Biol. 1279:79–95. doi:10.1007/978-1-4939-2398-4_6/COVER. [accessed 2022 Sep 26]. https://link.springer.com/protocol/10.1007/978-1-4939-2398-4_6.

Marquis JF, Nantel A, LaCourse R, Ryan L, North RJ, Gros P. 2008. Fibrotic response as a distinguishing feature of resistance and susceptibility to pulmonary infection with Mycobacterium tuberculosis in mice. Infect Immun. 76(1):78–88. doi:10.1128/IAI.00369-07. [accessed 2020 Aug 11]. /pmc/articles/PMC2223652/?report=abstract.

Medina E, North RJ. 1998. Resistance ranking of some common inbred mouse strains to Mycobacterium tuberculosis and relationship to major histocompatibility complex haplotype and Nrampl genotype. Immunology. 93:270–274.

Mishra BB, Lovewell RR, Olive AJ, Zhang G, Wang W, Eugenin E, Smith CM, Phuah JY, Long JE, Dubuke ML, et al. 2017. Nitric oxide prevents a pathogen-permissive granulocytic inflammation during tuberculosis. Nat Microbiol 2017 27. 2(7):1–11. doi:10.1038/nmicrobiol.2017.72. [accessed 2023 Feb 28].

https://www.nature.com/articles/nmicrobiol201772.

Mitsos LM, Cardon LR, Fortin A, Ryan L, LaCourse R, North RJ, Gros P. 2000. Genetic control of susceptibility to infection with Mycobacterium tuberculosis in mice. Genes Immun. 1(8):467–477. doi:10.1038/sj.gene.6363712. [accessed 2020 Aug 14]. www.nature.com/gene.

Mitsos LM, Cardon LR, Ryan L, LaCourse R, North RJ, Gros P. 2003. Susceptibility to tuberculosis: A locus on mouse chromosome 19 (Trl-4) regulates Mycobacterium tuberculosis replication in the lungs. Proc Natl Acad Sci U S A. 100(11):6610–6615. doi:10.1073/pnas.1031727100. [accessed 2021 Mar 16]. www.pnas.org.

Moreira-Teixeira L, Redford PS, Stavropoulos E, Ghilardi N, Maynard CL, Weaver CT, Freitas do Rosário AP, Wu X, Langhorne J, O'Garra A. 2017. T Cell–Derived IL-10 Impairs Host Resistance to Mycobacterium tuberculosis Infection . J Immunol. 199(2):613–623. doi:10.4049/jimmunol.1601340. [accessed 2021 Jul 3]. /pmc/articles/PMC5502318/.

Moreira-Teixeira L, Tabone O, Graham CM, Singhania A, Stavropoulos E, Redford PS, Chakravarty P, Priestnall SL, Suarez-Bonnet A, Herbert E, et al. 2020. Mouse transcriptome reveals potential signatures of protection and pathogenesis in human tuberculosis. Nat Immunol 2020 214. 21(4):464–476. doi:10.1038/s41590-020-0610-z. [accessed 2022 May 9]. https://www.nature.com/articles/s41590-020-0610-z.

Nambi S, Long JE, Mishra BB, Baker R, Murphy KC, Olive AJ, Nguyen HP, Shaffer SA, Sassetti CM. 2015. The Oxidative Stress Network of Mycobacterium tuberculosis Reveals Coordination between Radical Detoxification Systems. Cell Host Microbe. 17(6):829–837. doi:10.1016/j.chom.2015.05.008. [accessed 2021 May 18].

/pmc/articles/PMC4465913/.

Parker CC, Dickson PE, Philip VM, Thomas M, Chesler EJ. 2017. Systems Genetic Analysis in GeneNetwork.org. Curr Protoc Neurosci. 79(1):8.39.1-8.39.20. doi:10.1002/CPNS.23. [accessed 2023 Feb 16]. https://onlinelibrary.wiley.com/doi/full/10.1002/cpns.23.

Peirce JL, Lu L, Gu J, Silver LM, Williams RW. 2004. A new set of BXD recombinant inbred lines from advanced intercross populations in mice. BMC Genet. 5(1):1–17. doi:10.1186/1471-2156-5-7/FIGURES/4. [accessed 2022 Mar 24]. https://bmcgenomdata.biomedcentral.com/articles/10.1186/1471-2156-5-7.

Rosenberg OS, Dovey C, Tempesta M, Robbins RA, Finer-Moore JS, Stroud RM, Cox JS. 2011. EspR, a key regulator of Mycobacterium tuberculosis virulence, adopts a unique dimeric structure among helix-turn-helix proteins. Proc Natl Acad Sci U S A. 108(33):13450–13455. doi:10.1073/PNAS.1110242108/-/DCSUPPLEMENTAL. [accessed 2022 May 9]. /pmc/articles/PMC3158157/.

Roy S, Schmeier S, Kaczkowski B, Arner E, Alam T, Ozturk M, Tamgue O, Parihar SP, Kawaji H, Itoh M, et al. 2018. Transcriptional landscape of Mycobacterium tuberculosis infection in macrophages. Sci Rep. 8(1):1–7. doi:10.1038/S41598-018-24509-6. [accessed 2022 May 9]. /pmc/articles/PMC5928056/.

Sasani TA, Ashbrook DG, Beichman AC, Lu L, Palmer AA, Williams RW, Pritchard JK, Harris K. 2022. A natural mutator allele shapes mutation spectrum variation in mice. Nat 2022 6057910. 605(7910):497–502. doi:10.1038/s41586-022-04701-5. [accessed 2023 Feb 16]. https://www.nature.com/articles/s41586-022-04701-5.

Sassetti CM, Boyd DH, Rubin EJ. 2003. Genes required for mycobacterial growth

735 defined by high density mutagenesis. Mol Microbiol. 48(1):77–84. doi:10.1046/j.1365-
736 2958.2003.03425.x. [accessed 2021 Mar 19]. http://doi.wiley.com/10.1046/j.1365-
737 2958.2003.03425.x.
738 Sassetti CM, Rubin EJ. 2003. Genetic requirements for mycobacterial survival during
739 infection. Proc Natl Acad Sci U S A. 100(22):12989–12994.
740 doi:10.1073/pnas.2134250100. [accessed 2021 May 21]. /pmc/articles/PMC240732/.
741 Saul MC, Philip VM, Reinholdt LG, Chesler EJ. 2019. High-Diversity Mouse Populations
742 for Complex Traits. Trends Genet. 35(7):501–514. doi:10.1016/j.tig.2019.04.003.
743 [accessed 2021 Mar 16]. /pmc/articles/PMC6571031/.
744 Skelly DA, Czechanski A, Byers C, Aydin S, Spruce C, Olivier C, Choi K, Gatti DM,
745 Raghupathy N, Keele GR, et al. 2020. Mapping the Effects of Genetic Variation on
746 Chromatin State and Gene Expression Reveals Loci That Control Ground State
747 Pluripotency. Cell Stem Cell. 27(3):459-469.e8.
748 doi:10.1016/J.STEM.2020.07.005/ATTACHMENT/0B41E3B1-F882-4C29-B519-
749 DA741C0F9E18/MMC5.XLSX. [accessed 2022 Mar 24].
750 http://www.cell.com/article/S193459092030343X/fulltext.
751 Sklar JG, Makinoshima H, Schneider JS, Glickman MS. 2010. M. tuberculosis
752 intramembrane protease Rip1 controls transcription through three anti-sigma factor
753 substrates. Mol Microbiol. 77(3):605. doi:10.1111/J.1365-2958.2010.07232.X.
754 [accessed 2022 May 9]. /pmc/articles/PMC3008510/.
755 Smith CM, Baker RE, Proulx MK, Mishra BB, Long JE, Park SW, Lee HN, Kiritsy MC,
756 Bellerose MM, Olive AJ, et al. 2022. Host-pathogen genetic interactions underlie
757 tuberculosis susceptibility in genetically diverse mice. Elife. 11.

758 doi:10.7554/ELIFE.74419.

759 Smith CM, Sassetti CM. 2018. Modeling Diversity: Do Homogeneous Laboratory Strains
760 Limit Discovery? Trends Microbiol. 26(11):892–895. doi:10.1016/J.TIM.2018.08.002.
761 [accessed 2022 Mar 24]. http://www.cell.com/article/S0966842X18301744/fulltext.

762 Taylor B, Heiniger H, Meier H. 1973. Genetic Analysis of Resistance to Cadmium-
763 Induced Testicular Damage in Mice. Proc Soc Exp Biol Med.

764 Taylor BA, Wnek C, Kotlus BS, Roemer N, MacTaggart T, Phillips SJ. 1999.
765 Genotyping new BXD recombinant inbred mouse strains and comparison of BXD and
766 consensus maps. Mamm Genome 1999 104. 10(4):335–348.
767 doi:10.1007/S003359900998. [accessed 2022 Mar 24].
768 https://link.springer.com/article/10.1007/s003359900998.

769 Tsuyuguchi K, Suzuki K, Matsumoto H, Tanaka E, Amitani R, Kuze F. 2001. Effect of
770 oestrogen on Mycobacterium avium complex pulmonary infection in mice. Clin Exp
771 Immunol. 123(3):428. doi:10.1046/J.1365-2249.2001.01474.X. [accessed 2021 Aug
772 31]. /pmc/articles/PMC1906003/.

773 Wang R, Kreutzfeldt K, Botella H, Vaubourgeix J, Schnappinger D, Ehrt S. 2019.
774 Persistent mycobacterium tuberculosis infection in mice requires PerM for successful
775 cell division. Elife. 8. doi:10.7554/ELIFE.49570.

776 Wang X, Pandey AK, Mulligan MK, Williams EG, Mozhui K, Li Z, Jovaisaite V, Quarles
777 LD, Xiao Z, Huang J, et al. 2016. Joint mouse-human phenome-wide association to
778 test gene function and disease risk. doi:10.1038/ncomms10464. [accessed 2023 Feb
779 10]. www.genenetwork.org.

780 Whitaker M, Ruecker N, Hartman T, Klevorn T, Andres J, Kim J, Rhee K, Ehrt S. 2020.

781 Two interacting ATPases protect mycobacterium tuberculosis from glycerol and nitric
782 oxide toxicity. J Bacteriol. 202(16). doi:10.1128/JB.00202-
783 20/SUPPL_FILE/JB.00202-20-SD002.XLSX. [accessed 2022 Mar 24].
784 https://journals.asm.org/doi/full/10.1128/JB.00202-20.
785 WHO. 2022. Global Tuberculosis Report. :1–2.
786 Wu Y, Williams EG, Dubuis S, Mottis A, Jovaisaite V, Houten SM, Argmann CA, Faridi
787 P, Wolski W, Kutalik Z, et al. 2014. Multilayered genetic and omics dissection of
788 mitochondrial activity in a mouse reference population. Cell. 158(6):1415–1430.
789 doi:10.1016/J.CELL.2014.07.039/ATTACHMENT/4715B449-A909-458F-8FC8-
790 7424BC64964E/MMC2.XLSX. [accessed 2022 Mar 24].
791 http://www.cell.com/article/S0092867414009891/fulltext.
792 Yan BS, Kirby A, Shebzukhov Y V., Daly MJ, Kramnik I. 2006. Genetic architecture of
793 tuberculosis resistance in a mouse model of infection. Genes Immun. 7(3):201–210.
794 doi:10.1038/sj.gene.6364288. [accessed 2021 Mar 16].
795 https://pubmed.ncbi.nlm.nih.gov/16452998/.
796 Zak DE, Penn-Nicholson A, Scriba TJ, Thompson E, Suliman S, Amon LM, Mahomed
797 H, Erasmus M, Whatney W, Hussey GD, et al. 2016. A blood RNA signature for
798 tuberculosis disease risk: a prospective cohort study. Lancet. 387(10035):2312–
799 2322. doi:10.1016/S0140-6736(15)01316-1. [accessed 2020 Sep 12].
800 https://pubmed.ncbi.nlm.nih.gov/27017310/.
801 Zhang J, Lan Y, Li MY, Lamers MM, Fusade-Boyer M, Klemm E, Thiele C, Ashour J,
802 Sanyal S. 2018. Flaviviruses Exploit the Lipid Droplet Protein AUP1 to Trigger
803 Lipophagy and Drive Virus Production. Cell Host Microbe. 23(6):819-831.e5.

804 doi:10.1016/J.CHOM.2018.05.005/ATTACHMENT/AD40031E-B931-4DFA-91D0-

805 55A3B36F64F6/MMC3.XLSX. [accessed 2022 May 9].

806 http://www.cell.com/article/S1931312818302592/fulltext.

807

808

Table 1: Genome-wide significant QTL (p ≤ 0.05). "*hp*QTL" is the name for each host-pathogen QTL of genome-wide significance (p ≤ 0.05). "Trait" refers to the Rv number of the bacterial mutant whose fitness profile identified the *hp*QTL in the host genome. "Gene" is the bacterial gene annotation of the mutant if one is available on Mycobrowser. "Chr" is the host chromosome on which the QTL is located, and "Position (Mb)" is the position of the QTL in megabases. "LOD" is the maximum association score between the mutant fitness profile and the host locus. "Start (Mb)" and "End (Mb)" are the lower and upper boundaries of the Bayesian 95% confidence interval. "P-value" denotes the significance of the association between the bacterial mutant fitness and the host genetic locus.

hpQTL	Trait	Gene	Chr	Position (Mb)	LOD	Start (Mb)	End (Mb)	P-value
hp001	Rv0913c	Rv0913c	1	22.773	3.52	5.022	73.222	2.24E-02
hp002	Rv0778	cyp126	1	121.148	3.98	115.474	126.340	1.67E-02
hp003	Rv2468c	Rv2468c	1	152.965	4.54	147.055	166.299	2.33E-02
hp004	Rv1260	Rv1260	1	155.701	4.29	143.711	160.273	3.94E-02
hp005	Rv0103c	ctpB	1	189.196	3.09	3.010	195.308	4.60E-02
hp006	Rv1525	wbbL2	2	10.808	3.56	5.653	14.395	3.32E-02
hp007	Rv3400	Rv3400	2	24.076	4.12	17.898	42.375	8.38E-03
hp008	Rv0625c	Rv0625c	2	45.533	3.37	25.645	161.538	5.01E-02
hp009	Rv0599c	vapB27	2	46.212	3.74	42.557	54.975	7.86E-03
hp010	Rv3294c	Rv3294c	2	138.850	3.56	136.128	158.741	3.73E-02
hp011	Rv3565	aspB	2	159.316	3.88	42.557	174.820	1.47E-02
hp012	Rv2546	vapC18	2	169.114	4.90	168.446	169.887	1.80E-03
hp013	Rv1965	yrbE3B	2	170.362	3.50	15.435	180.835	1.43E-02
hp014	Rv1367c	Rv1367c	2	173.385	3.77	46.133	176.951	1.85E-02
hp015	Rv1290A	Rv1290A	2	181.009	2.96	14.698	181.991	2.36E-02
hp016	Rv3047c	Rv3047c	3	41.212	3.92	39.644	51.561	4.49E-02
hp017	Rv0101	nrp	3	57.642	3.69	42.035	61.219	6.19E-03
hp018	Rv2051c	ppm1	3	62.392	4.25	61.219	70.185	1.94E-02
hp019	Rv1935c	echA13	3	129.496	4.23	10.997	157.792	4.20E-02
hp020	Rv1735c	Rv1735c	3	129.508	3.64	117.504	157.140	4.20E-02
hp021	Rv2602	vapC41	3	132.174	4.01	129.509	138.245	1.12E-02

hp022	Rv0773c	ggtA	3	146.239	4.56	143.570	156.034	2.75E-02
hp023	Rv0077c	Rv0077c	4	144.942	4.31	144.913	148.864	1.04E-02
hp024	Rv0588	yrbE2B	4	153.793	3.76	54.951	155.498	3.23E-02
hp025	Rv0093c	Rv0093c	5	28.411	3.05	19.137	132.038	2.29E-02
hp026	Rv0768	aldA	5	43.085	4.19	29.537	52.408	3.09E-03
hp027	Rv2957	Rv2957	5	117.550	3.27	3.143	139.501	3.26E-02
hp028	Rv3848	Rv3848	5	136.015	5.69	133.911	138.657	1.55E-02
hp029	Rv0359	rip2	6	76.492	4.18	75.970	82.500	5.63E-03
hp030	Rv0955	perM	6	82.500	4.80	80.286	83.092	1.29E-02
hp031	Rv2140c	TB18.6	6	84.277	4.62	80.286	85.650	2.28E-02
hp032	Rv3849	espR	6	84.869	6.77	83.684	85.566	6.23E-03
hp033	Rv0127	mak	6	85.650	7.83	84.277	88.578	7.04E-03
hp034	Rv1056	Rv1056	6	93.600	4.10	89.371	95.127	4.40E-02
hp035	Rv2671	ribD	6	148.818	3.53	12.797	149.266	1.60E-02
hp036	Rv3711c	dnaQ	7	27.300	3.31	24.735	145.321	3.80E-02
hp037	Rv3299c	atsB	7	36.692	3.01	3.078	144.446	5.34E-02
hp038	Rv0065	vapC1	7	37.008	3.41	3.078	144.445	4.72E-02
hp039	Rv1530	adh	7	37.008	3.22	3.078	145.321	3.74E-02
hp040	Rv2482c	plsB2	7	37.008	3.55	24.619	144.445	2.35E-02
hp041	Rv0026	Rv0026	7	37.760	3.34	24.764	128.756	2.82E-02
hp042	Rv1913	Rv1913	7	39.822	3.63	30.689	145.321	2.96E-03
hp043	Rv1236	sugA	7	40.289	3.13	24.822	140.297	5.28E-03
hp044	Rv1528c	papA4	7	40.289	4.97	40.226	46.357	2.11E-02
hp045	Rv1542c	glbN	7	40.289	3.71	3.078	145.321	5.77E-02
hp046	Rv1992c	ctpG	7	40.289	3.24	6.015	145.321	3.20E-02
hp047	Rv3702c	Rv3702c	7	40.289	4.55	24.793	140.297	2.75E-02
hp048	Rv2388c	hemN	7	84.014	3.39	39.894	127.779	2.54E-02
hp049	Rv0852	fadD16	7	97.465	3.71	83.879	128.058	3.89E-02
hp050	Rv0878c	PPE13	7	97.685	4.10	89.870	127.500	2.49E-02
hp051	Rv0089	Rv0089	7	116.709	4.08	98.124	127.989	3.64E-02
hp052	Rv1912c	fadB5	7	134.484	4.49	51.060	134.831	1.14E-02
hp053	Rv3868	eccA1	7	134.598	3.80	17.136	144.445	4.40E-02
hp054	Rv2637	dedA	7	140.297	4.63	138.137	140.586	1.63E-02
hp055	Rv0271c	fadE6	7	140.586	5.74	140.586	143.684	3.53E-02
hp056	Rv1984c	cfp21	7	140.586	3.44	24.938	144.445	1.68E-02
hp057	Rv1104	Rv1104	7	143.809	3.29	24.735	145.321	2.49E-02
hp058	Rv3179	Rv3179	7	143.809	3.78	140.586	144.445	5.34E-02
hp059	Rv1748	Rv1748	7	144.184	5.42	37.760	144.446	7.25E-03
hp060	Rv3288c	usfY	7	144.184	3.97	30.593	145.321	3.46E-02

hp061	Rv3698	Rv3698	7	144.309	3.41	12.026	145.321	3.60E-02
hp062	Rv1245c	Rv1245c	7	144.446	3.97	40.289	145.321	2.62E-03
hp063	Rv2092c	helY	7	144.687	5.34	144.533	145.321	2.50E-02
hp064	Rv0458	Rv0458	7	145.321	3.92	144.448	145.321	2.93E-02
hp065	Rv0538	Rv0538	8	11.279	4.57	11.279	13.680	1.47E-02
hp066	Rv2066	cobI	8	14.819	4.31	12.880	15.343	4.00E-02
hp067	Rv1039c	PPE15	8	16.687	4.55	13.680	16.946	1.31E-02
hp068	Rv3855	ethR	8	87.897	4.62	87.219	89.367	1.44E-02
hp069	Rv2161c	Rv2161c	8	113.708	4.09	109.407	128.590	5.93E-03
hp070	Rv2384	mbtA	9	29.939	4.02	4.359	107.777	3.24E-02
hp071	Rv1954c	Rv1954c	9	34.618	4.70	29.941	58.854	2.24E-02
hp072	Rv3899c	Rv3899c	9	94.905	4.16	87.462	101.324	3.61E-02
hp073	Rv0950c	Rv0950c	9	101.365	3.92	4.359	106.019	2.64E-02
hp074	Rv0538	Rv0538	9	103.686	4.05	80.003	106.019	4.83E-02
hp075	Rv3087	Rv3087	10	5.031	4.52	3.181	9.092	3.38E-02
hp076	Rv2529	Rv2529	10	9.413	4.33	3.181	11.991	9.41E-03
hp077	Rv1450c	PE_PGRS27	10	19.780	4.04	13.853	21.509	3.92E-02
hp078	Rv1507c	Rv1507c	10	55.483	4.97	55.356	59.293	1.73E-02
hp079	Rv1366	Rv1366	10	64.014	3.25	57.276	72.506	2.31E-02
hp080	Rv1552	frdA	10	96.749	3.97	95.639	103.562	3.45E-02
hp081	Rv1753c	PPE24	10	109.165	3.52	13.688	127.327	1.75E-02
hp082	Rv2261c	Rv2261c	10	111.074	4.75	110.998	126.607	1.16E-02
hp083	Rv0044c	Rv0044c	10	115.897	3.42	3.181	127.808	6.21E-02
hp084	Rv2326c	Rv2326c	10	120.610	4.29	116.134	121.419	1.26E-02
hp085	Rv0769	Rv0769	10	126.740	4.12	123.469	126.808	2.36E-02
hp086	Rv2993c	Rv2993c	11	11.620	4.35	8.814	15.810	3.65E-02
hp087	Rv3759c	proX	11	21.073	4.70	19.834	34.416	4.71E-02
hp088	Rv0086	hycQ	11	24.850	3.37	18.284	35.583	1.22E-02
hp089	Rv3841	bfrB	11	47.049	3.28	35.903	80.586	1.67E-02
hp090	Rv0126	treS	11	65.541	3.56	64.895	81.165	3.85E-02
hp091	Rv2116	lppK	11	73.243	4.46	73.194	81.165	1.67E-02
hp092	Rv0765c	Rv0765c	11	106.661	4.70	106.040	107.457	2.58E-02
hp093	Rv1850	ureC	11	107.742	4.25	107.422	110.228	1.61E-02
hp094	Rv2802c	Rv2802c	11	107.742	4.87	107.133	109.751	9.90E-03
hp095	Rv1452c	PE_PGRS28	11	107.964	3.29	103.707	111.341	4.10E-02
hp096	Rv0599c	vapB27	11	113.557	3.58	110.546	118.682	1.76E-02
hp097	Rv1969	mce3D	12	46.628	4.14	27.823	52.908	4.09E-02
hp098	Rv3554	fdxB	12	71.873	3.22	58.970	114.110	4.64E-02
hp099	Rv1448c	tal	12	79.511	4.90	76.378	86.909	1.38E-02

hp100	Rv2922c	smc	12	105.499	4.57	104.281	107.191	3.70E-02
hp101	Rv2268c	cyp128	12	107.369	3.62	5.594	107.848	3.59E-02
hp102	Rv1775	Rv1775	12	108.105	3.71	107.369	108.898	3.33E-02
hp103	Rv3164c	moxR3	12	114.166	4.13	111.180	116.685	3.60E-02
hp104	Rv2019	Rv2019	13	6.304	3.82	4.432	115.537	4.09E-02
hp105	Rv2379c	mbtF	13	18.035	3.66	4.432	45.238	3.69E-02
hp106	Rv0066c	icd2	13	39.372	4.40	34.110	39.515	1.60E-02
hp107	Rv1250	Rv1250	13	50.000	3.82	45.902	54.614	2.04E-02
hp108	Rv2282c	Rv2282c	13	54.862	3.93	54.843	72.958	3.30E-02
hp109	Rv2074	Rv2074	13	63.704	5.16	61.332	71.002	6.80E-03
hp110	Rv0552	Rv0552	13	67.497	5.30	63.792	67.497	3.26E-02
hp111	Rv1009	rpfB	13	75.762	4.75	72.969	84.394	2.23E-02
hp112	Rv0223c	Rv0223c	14	73.646	4.05	73.198	79.374	2.12E-02
hp113	Rv3063	cstA	14	79.403	3.63	61.301	118.199	1.55E-02
hp114	Rv1525	wbbL2	15	27.520	3.75	11.145	102.347	1.79E-02
hp115	Rv3013	Rv3013	15	28.265	3.98	12.673	28.312	1.65E-02
hp116	Rv3354	Rv3354	15	28.312	2.83	9.237	102.347	4.35E-02
hp117	Rv1664	pks9	15	32.262	2.86	7.168	72.449	3.57E-02
hp118	Rv1366	Rv1366	15	64.513	3.43	42.380	84.022	9.72E-03
hp119	Rv3765c	tcrX	15	74.502	4.19	69.446	75.001	6.29E-03
hp120	Rv0454	Rv0454	15	75.750	4.13	75.001	82.088	1.87E-02
hp121	Rv2315c	Rv2315c	15	84.037	3.37	7.814	102.354	4.37E-02
hp122	Rv0242c	fabG4	15	88.975	5.10	86.329	90.948	5.91E-03
hp123	Rv0959	Rv0959	15	91.863	4.47	90.948	93.408	4.13E-02
hp124	Rv1961	Rv1961	15	95.169	4.46	94.529	96.191	5.17E-02
hp125	Rv0043c	Rv0043c	16	44.080	3.98	36.743	44.128	2.51E-02
hp126	Rv1400c	lipI	16	78.088	3.52	75.905	85.637	3.92E-02
hp127	Rv1552	frdA	16	92.557	3.95	74.904	96.503	3.60E-02
hp128	Rv3058c	Rv3058c	17	55.278	4.32	6.007	76.812	2.40E-04
hp129	Rv1507A	Rv1507A	17	85.527	4.44	80.477	87.364	6.91E-03
hp130	Rv3776	Rv3776	17	94.132	4.63	91.701	94.411	1.16E-02
hp131	Rv3495c	lprN	18	57.375	4.87	57.348	58.270	3.71E-02
hp132	Rv1084	Rv1084	19	10.714	4.90	3.337	14.209	2.73E-02
hp133	Rv2378c	mbtG	19	23.841	3.02	21.915	27.750	3.72E-02
hp134	Rv0056	rplI	19	39.978	4.00	38.651	42.427	3.83E-02
hp135	Rv3540c	ltp2	X	101.772	4.43	80.056	115.391	3.14E-03
hp136	Rv0694	lldD1	X	115.365	3.91	102.867	167.395	3.70E-02
hp137	Rv1791	PE19	X	119.825	4.38	115.497	128.620	2.38E-02
hp138	Rv2733c	Rv2733c	X	133.591	3.40	115.471	138.012	3.90E-02

hp139	Rv0182c	sigG	X	136.470	4.68	136.304	138.007	1.61E-02
hp140	Rv1413	Rv1413	X	138.012	4.90	135.586	139.435	5.84E-03

Figure Legends

Figure 1: B6 and D2 are phenodeviant in TB susceptibility. (**A**) Log_{10} transformed colony forming units (CFU) recovered from lung tissue throughout the course of the aerosol infection (with an infectious dose of ~40 CFU of *Mtb* H37Rv). (**B**) Log_{10} transformed CFU recovered from spleen throughout infection. (**C** & **D**) Male B6 and D2 H&E-stained lung sections taken 6 weeks post-infection, 2X magnification, representative of n = 4 per genotype. Corresponding female sections can be found in **Figure S1C** & **D**. (**E**) Lung damage was quantified by QuPath v0.3.2 using an artificial neural network-based damage identification model and reported as a percent of total lung section area (n = 4 per genotype & sex). Lung damage is not significantly different between B6 and D2 at 6 weeks post-infection by unpaired Student's *t*-test. (**F** & **G**) Male B6 and D2 H&E-stained lung sections taken 12 weeks post-infection, 2X magnification, representative of n = 4 per genotype. Corresponding female sections can be found in **Figure S1E** & **F**. (**H**) Lung damage, quantified as in **E**, is significantly different between B6 and D2 at 12 weeks post-infection by unpaired Student's *t*-test.

Figure 2: BXD panel exhibits natural genetic variation, but classical clinical traits cannot map genome-wide QTL at 4 weeks post-infection. (**A**) The BXD panel is a biparental recombinant inbred panel bred from C57BL/6J (B6) and DBA/2J (D2) and composed of over 100 mosaic strains. (**B**) Lung and spleen burden by host genotype (n

= 1-5 per genotype). (**C**) QTL mapping of lung and spleen burden traits across the BXD cohort. Solid threshold represents a genome-wide significance of p = 0.05. Dashed threshold represents p = 0.20. Thresholds were calculated from 10,000 permutation tests.

Figure 3: TnSeq mutant fitness is a sensitive reporter of the factors that drive disease outcome. (**A**) Multiple mice from each BXD and parental strain were infected with 10^6 CFU of *Mtb* TnSeq library, representative of ~10^5 independent *Mtb* transposon mutants. For each mutant, the change between the initial abundance in the TnSeq library and the abundance recovered after 4 weeks of *in vivo* infection was compared to calculate a quantitative fitness metric (log_2 fold change; LFC), which could be used downstream for QTL mapping. (**B**) Example plot showing an essential *Mtb* gene (*bioA*), a conditionally essential gene (*mbtG*), and a non-essential gene (*glpK*) across the BXD panel. (**C**) A Venn diagram depicting the overlap of essential genes between B6, D2, and the screened BXD strains. *Mtb* genes were deemed essential if the transposon mutant experienced a one-fold reduction (LFC < -0.5) within a given host genotype and were significantly different from *in vitro* conditions (p < 0.05) in at least one host genotype across the panel. (**D**) The number of *Mtb* genes essential (LFC < -0.5) for growth or survival in each diverse mouse strain across the panel (p < 0.05). Salmon indicates the mutants uniquely required for each host additional strain, and purple shows the cumulative requirement as each new host strain is added. (**E**) A heatmap depicting the total correlation of the library-wide bacterial fitness within each screened host strain.

Figure 4: TnSeq mutant fitness endophenotypes map genome-wide significant QTL. (**A**) The QTL that reach a significance threshold of p ≤ 0.01. The color of the QTL corresponds to the Mycobrowser class of the gene absent from the transposon mutant that mapped the QTL. The width of each segment corresponds to the size of the 95% Bayesian confidence interval of the QTL. (**B**) A pie chart tabulating the Mycobrowser classes of the mutants that mapped highly significant QTL (p ≤ 0.01), beyond the genome-wide significance threshold of p ≤ 0.05.

Figure 5: A chromosome 6 QTL hotspot highlights a genomic region controlling fitness of multiple bacterial mutants. QTL mapping of transposon mutants lacking (**A**) *mak,* (**B**) *espR*, (**C**) *perM*, and (**D**) *rip2*. After 10,000 permutation tests, the solid threshold represents p = 0.05, and the dashed threshold represents p = 0.20. (**E**) Chromosome 6 mapping overlap of the four transposon mutant fitness profiles that identified the QTL hotspot. (**F**-**I**) Boxplots representing the fitness of transposon mutants lacking *mak, espR*, *perM*, and *rip2* within BXD mice with *B* (navy) or *D* (lilac) haplotypes at the QTL position. BXD genotypes for which a haplotype state could not be called with 95% confidence were not included.

Figure 6: Independence tests identify two putative causal variants. Scan2 independence tests from R/qtl were used to identify whether the chromosome 6 hotspot may represent more than one causal locus. The QTL mapped by *mak* (**A**), *espR* (**B**), *perM* (**C**), and *rip2* (**D**) transposon mutants were remapped, incorporating the haplotype

887 of the BXD mice at the locus of each other QTL as a covariate in the mapping analysis.
888 The original QTL mapped by each mutant fitness profile are represented as dashed
889 lines. The solid horizontal threshold represents p = 0.05 while the dashed horizontal
890 threshold represents p = 0.20.
891
892 **Figure 7: A bioinformatic pipeline highlights putative candidate genes underlying**
893 **the QTL on chromosome 6.** (**A**) A graphic summarizing the bioinformatic pipeline used
894 to prioritize host gene candidates within each QTL. (**B**) A heatmap representative of the
895 per-gene outcome of five distinct criteria: *i)* whether or not D2 possesses a missense or
896 nonsense mutation in comparison to B6 according to the Wellcome Sanger Institute
897 Mouse Genomes Project (Sanger MGP) (Adams et al. 2015), *ii)* whether the gene is
898 significantly enriched in genetically diverse mice progressively infected with *Mtb* (Ahmed
899 et al. 2020), *iii)* whether the gene is significantly enriched in Rhesus Macaques
900 progressively infected with *Mtb* (Ahmed et al. 2020), *iv)* whether the gene is significantly
901 up- or downregulated in TB patient blood (Zak et al. 2016), and *v)* whether the gene is
902 differentially expressed in mouse lungs across variable host genotypes, *Mtb* genotypes,
903 and doses (Moreira-Teixeira et al. 2020). If the answer is no, the space remains blank.
904 Green indicates yes, and yellow indicates yes but cautions that the Rhesus Macaque
905 gene is not a high confidence homolog. Only protein coding genes with a D2 SNP (as
906 per Sanger MGP) that met at least one of the criteria are included in this visual.

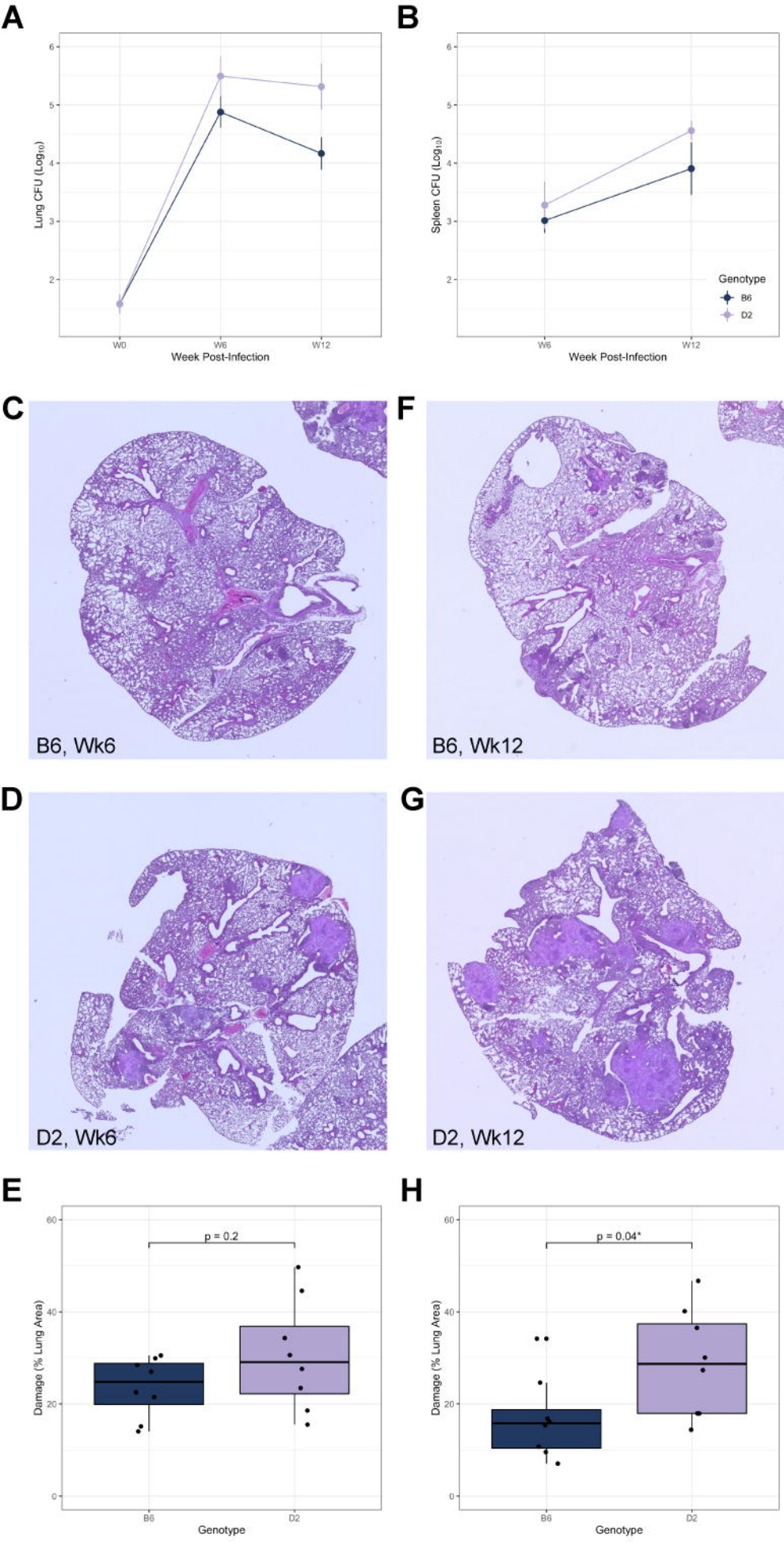
A
Lung CFU (Log10)
6
5
4
3
2
W0
W6
W12
Week Post-Infection
B
Spleen CFU (Log10)
6
5
4
3
2
W6
W12
Week Post-Infection
Genotype
B6
D2
C
B6, Wk6
F
B6, Wk12
D
D2, Wk6
G
D2, Wk12
E
Damage (% Lung Area)
60
40
20
0
p = 0.2
B6
D2
Genotype
H
Damage (% Lung Area)
60
40
20
0
p = 0.04*
B6
D2
Genotype

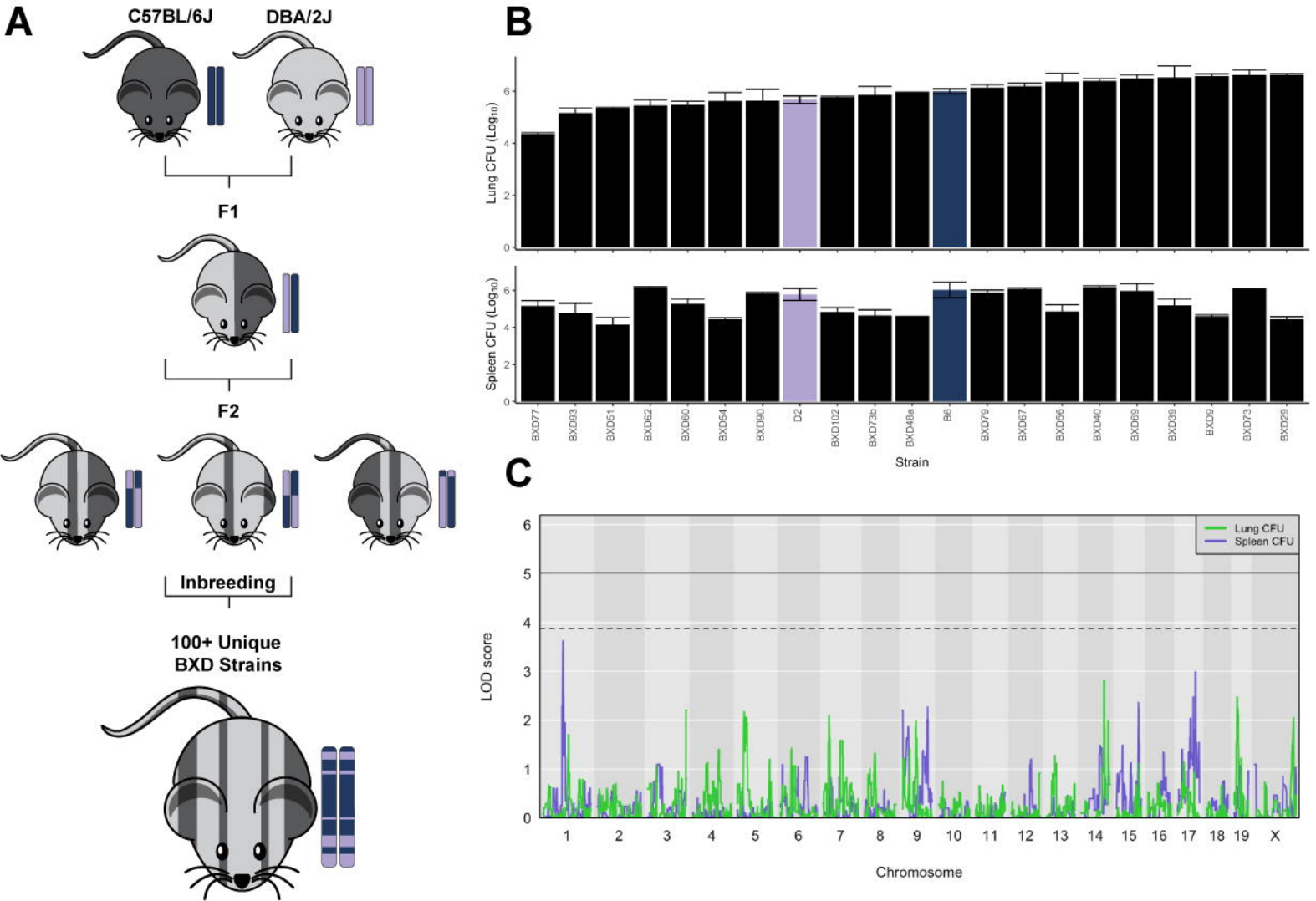
A
C57BL/6J
DBA/2J
F1
F2
Inbreeding
100+ Unique
BXD Strains
B
Lung CFU (Log10)
Spleen CFU (Log10)
BXD77
BXD93
BXD51
BXD62
BXD60
BXD54
BXD90
D2
BXD102
BXD73b
BXD48a
B6
BXD79
BXD67
BXD56
BXD40
BXD69
BXD39
BXD9
BXD73
BXD29
Strain
C
Lung CFU
Spleen CFU
LOD score
Chromosome

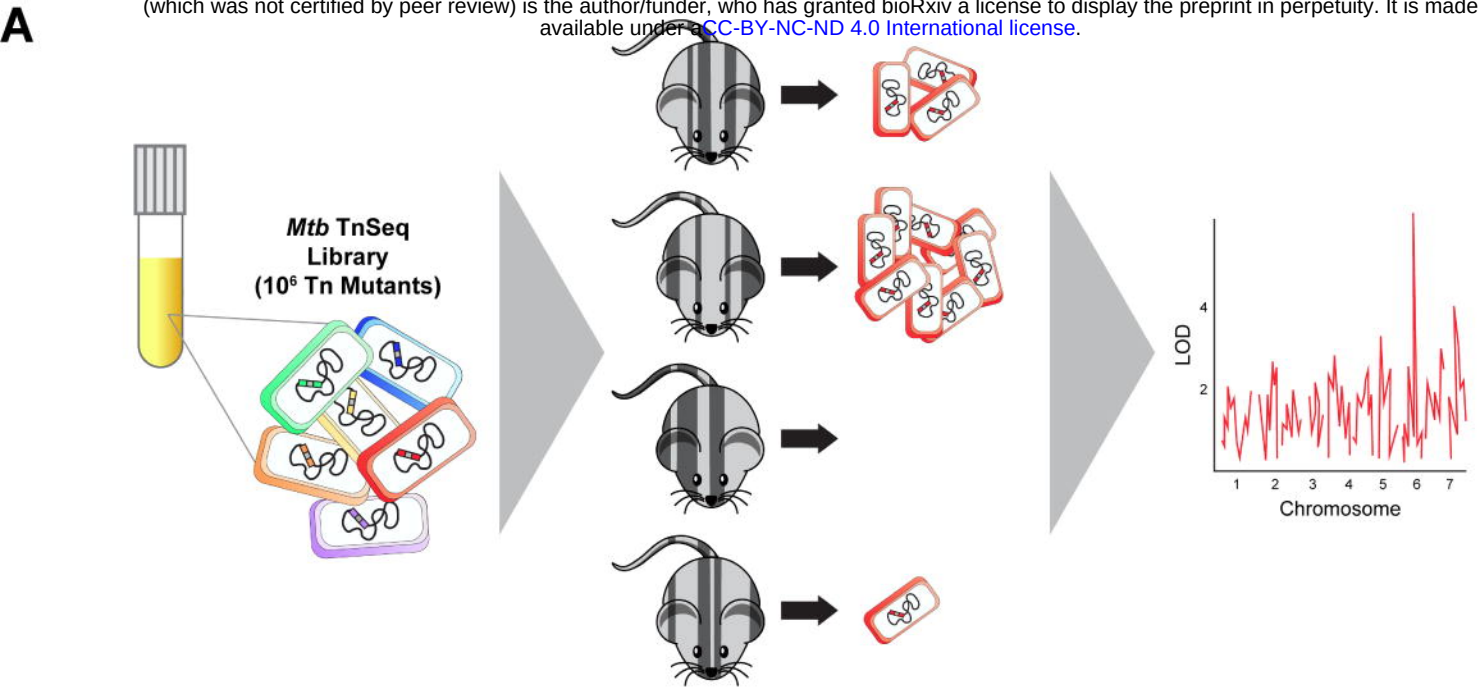

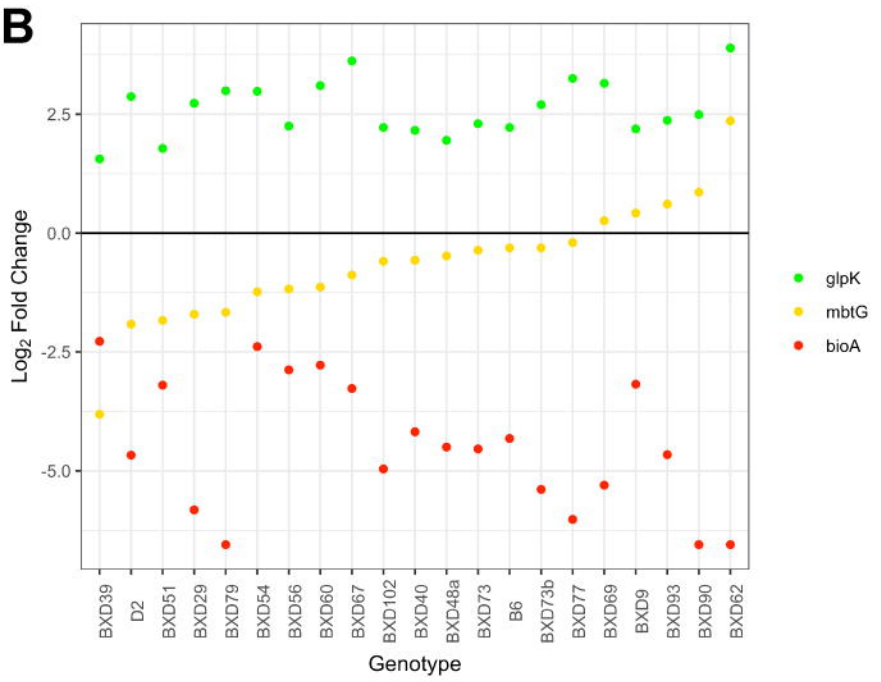

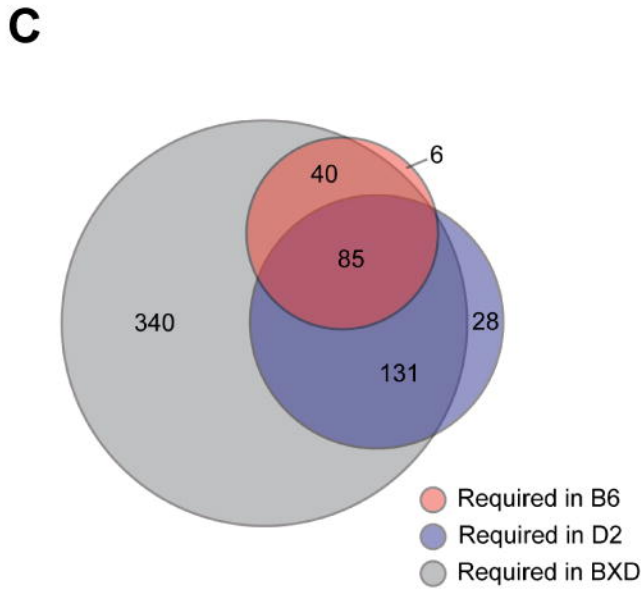

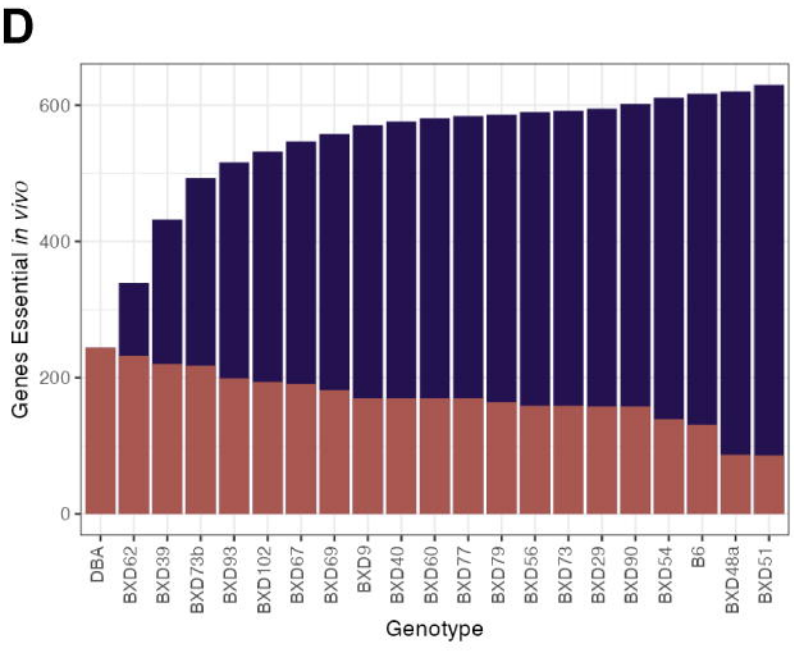

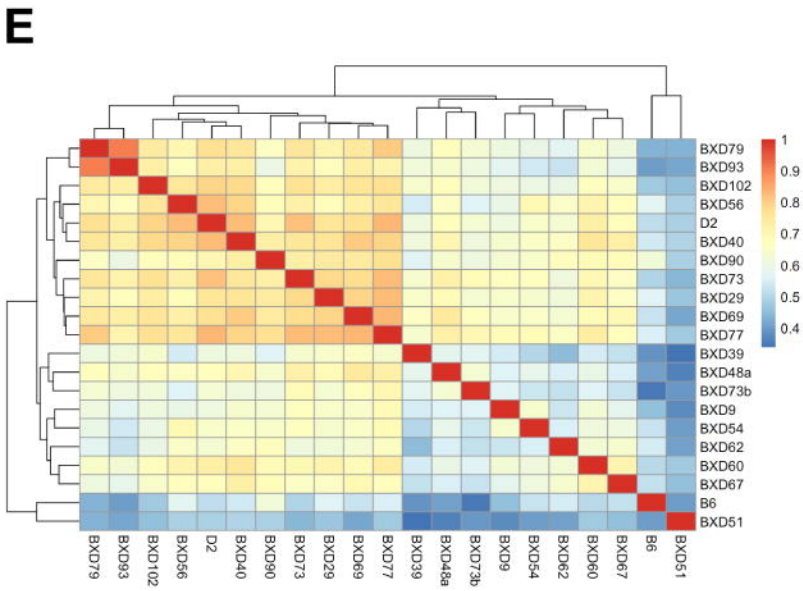

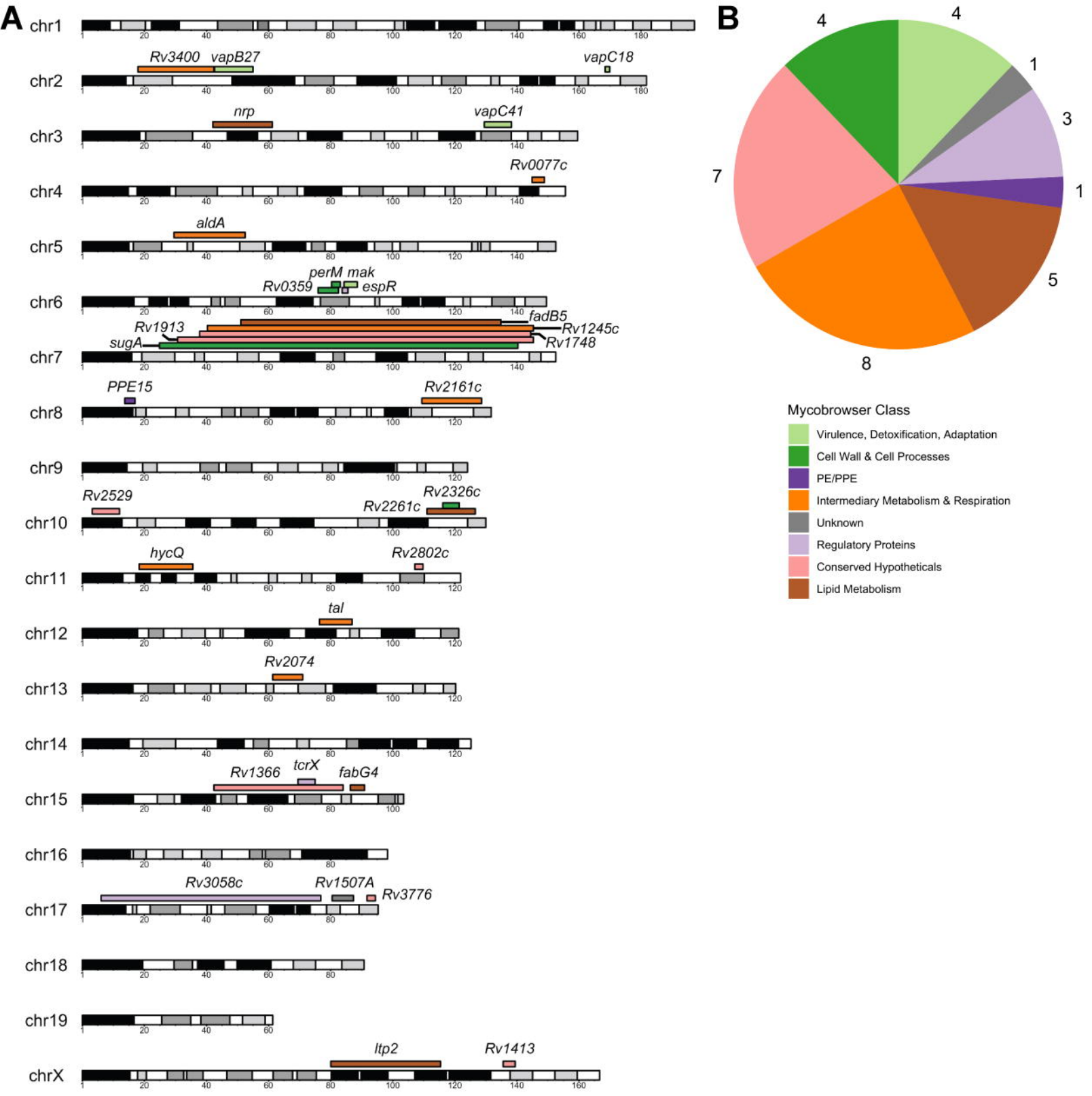
A
chr1
chr2
Rv3400
vapB27
vapC18
chr3
nrp
vapC41
chr4
Rv0077c
chr5
aldA
chr6
perM
mak
Rv0359
espR
chr7
fadB5
Rv1913
Rv1245c
sugA
Rv1748
chr8
PPE15
Rv2161c
chr9
chr10
Rv2529
Rv2326c
Rv2261c
chr11
hycQ
Rv2802c
chr12
tal
chr13
Rv2074
chr14
chr15
Rv1366
tcrX
fabG4
chr16
chr17
Rv3058c
Rv1507A
Rv3776
chr18
chr19
chrX
ltp2
Rv1413
B
4
4
1
3
1
5
8
7
Mycobrowser Class
Virulence, Detoxification, Adaptation
Cell Wall & Cell Processes
PE/PPE
Intermediary Metabolism & Respiration
Unknown
Regulatory Proteins
Conserved Hypotheticals
Lipid Metabolism

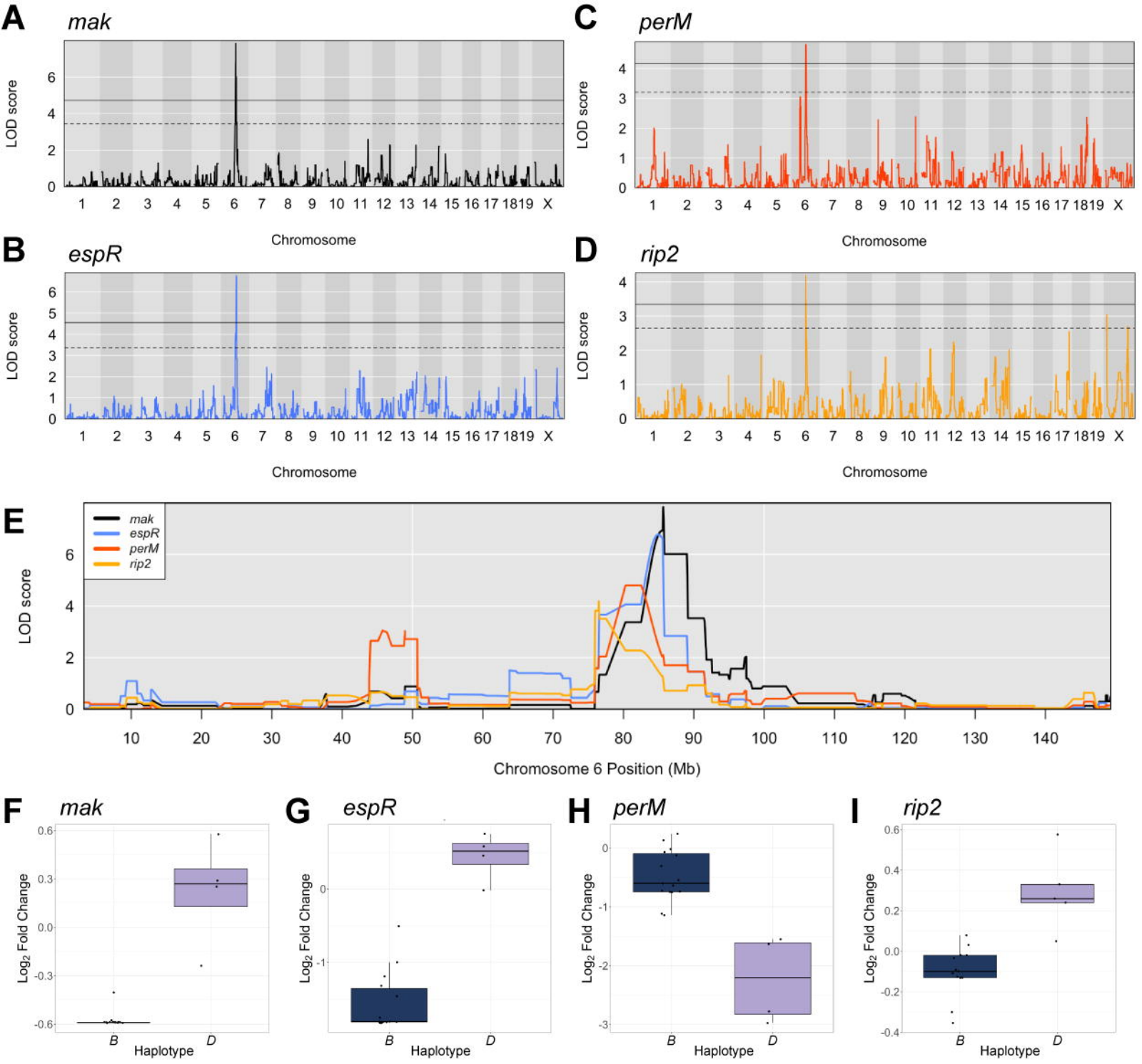
A
mak
LOD score
Chromosome
B
espR
C
perM
D
rip2
E
mak
espR
perM
rip2
Chromosome 6 Position (Mb)
F
mak
G
espR
H
perM
I
rip2
Log2 Fold Change
Haplotype
B
D

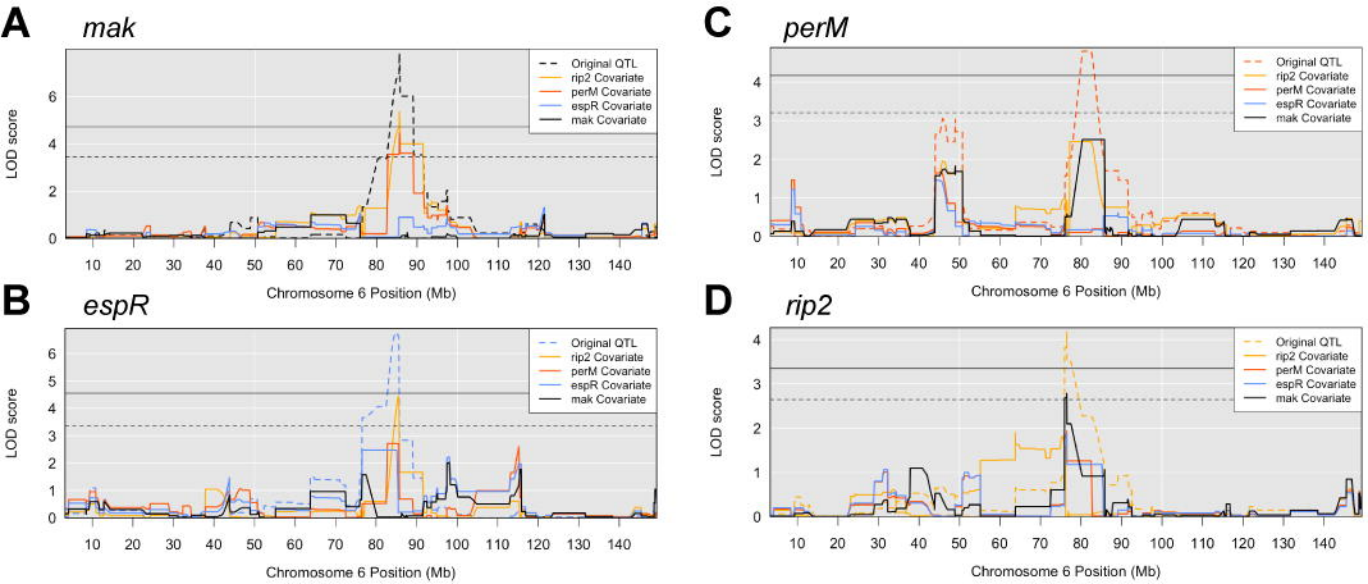
A
mak
B
espR
C
perM
D
rip2
Original QTL
rip2 Covariate
perM Covariate
espR Covariate
mak Covariate
LOD score
Chromosome 6 Position (Mb)

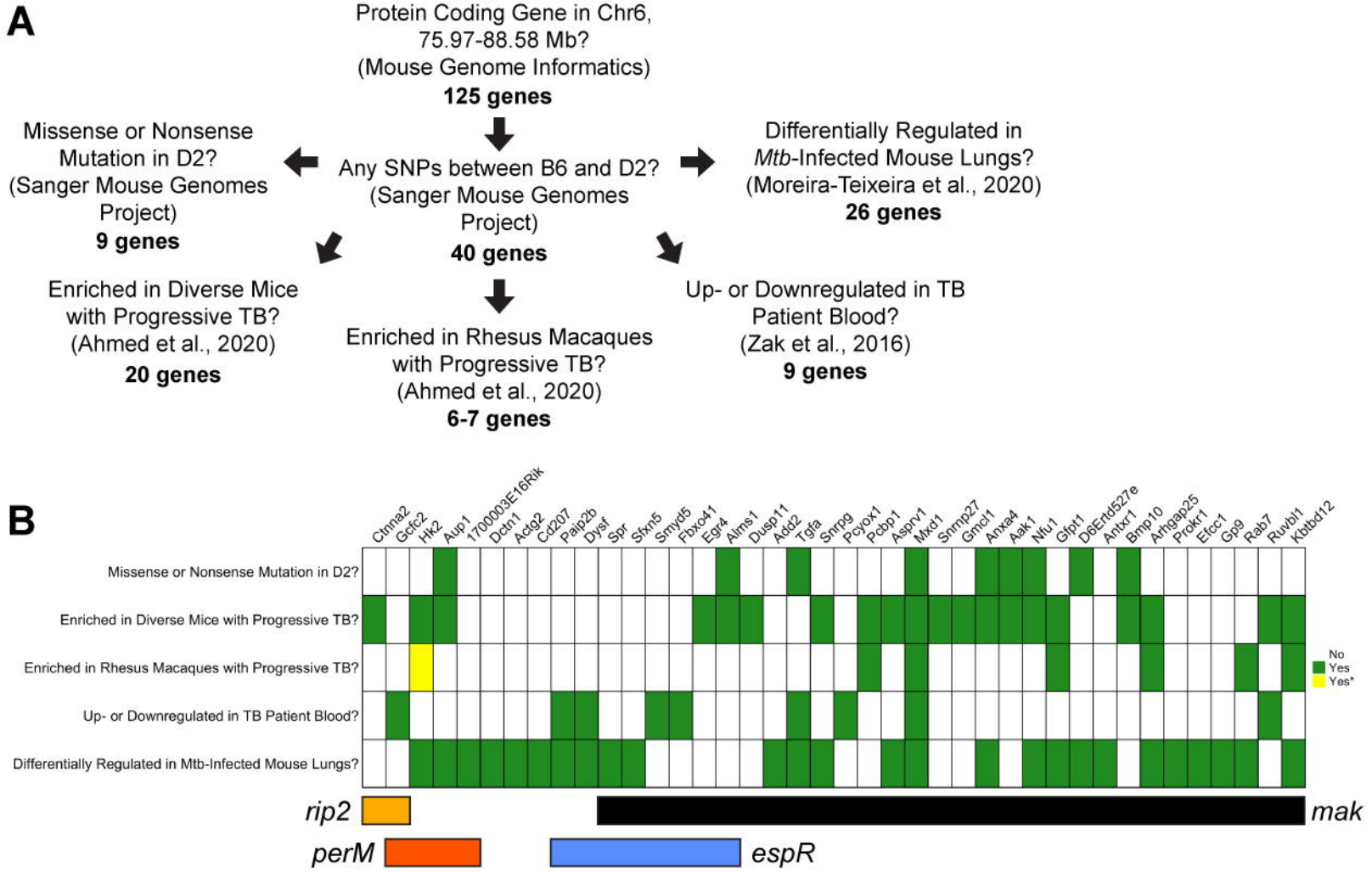
A
Protein Coding Gene in Chr6, 75.97-88.58 Mb? (Mouse Genome Informatics)
125 genes
Missense or Nonsense Mutation in D2? (Sanger Mouse Genomes Project)
9 genes
Any SNPs between B6 and D2? (Sanger Mouse Genomes Project)
40 genes
Differentially Regulated in Mtb-Infected Mouse Lungs? (Moreira-Teixeira et al., 2020)
26 genes
Enriched in Diverse Mice with Progressive TB? (Ahmed et al., 2020)
20 genes
Enriched in Rhesus Macaques with Progressive TB? (Ahmed et al., 2020)
6-7 genes
Up- or Downregulated in TB Patient Blood? (Zak et al., 2016)
9 genes
B
Ctnna2 Gcfc2 Hk2 Aup1 1700003E16Rik Dctn1 Actg2 Cd207 Paip2b Dysf Spr Sfxn5 Smyd5 Fbxo41 Egr4 Alms1 Dusp11 Add2 Tgfa Snrpg Pcyox1 Pcbp1 Asprv1 Mxd1 Snrnp27 Gmcl1 Anxa4 Aak1 Nfu1 Gfpt1 D6Ertd527e Antxr1 Bmp10 Arhgap25 Prokr1 Efcc1 Gp9 Rab7 Ruvbl1 Kbtbd12
Missense or Nonsense Mutation in D2?
Enriched in Diverse Mice with Progressive TB?
Enriched in Rhesus Macaques with Progressive TB?
Up- or Downregulated in TB Patient Blood?
Differentially Regulated in Mtb-Infected Mouse Lungs?
No
Yes
Yes*
rip2
mak
perM
espR